Journal of Controlled Release 398 (2026) 115227

Contents lists available at ScienceDirect

Journal of Controlled Release

journal homepage: www.elsevier.com/locate/jconrel

Quercetin-loaded bioinspired soy protein isolate-zein delivery system enabling pest management and plant growth promotion in sustainable agriculture

Keke Xiao, Wing-Fu Lai *

School of Food Science and Nutrition, University of Leeds, Leeds LS2 9JT, United Kingdom

ARTICLE INFO

Keywords:
Sustainable agriculture
Controlled release
Plant protein
Pest management
Crop enhancement

ABSTRACT

Strategies that reduce dependence on synthetic pesticides while maintaining crop productivity are increasingly emphasized in sustainable agriculture. Here, we developed a bioinspired plant protein-based delivery system consisting of quercetin-loaded soy protein isolate (SPI)-zein nanocapsules. Spray drying was employed as a structural engineering strategy to assemble and immobilize nanocapsules into pomegranate-like hierarchical particulate aggregates. SEM, fluorescence spectroscopy, FTIR, UV–vis spectroscopy, XRD and TGA were adopted to characterise quercetin-loaded SPI-zein systems prepared at different SPI:zein ratios. Structural and morphological analyses revealed spherical nanocapsules embedded within interconnected protein aggregates. The formulation with an SPI:zein ratio of 1:2 exhibited the best overall performance, including an encapsulation efficiency of 75.2%, loading capacity of 3.23%, pH-responsive release behaviour, enhanced rainfastness, and improved photochemical and storage stability. Notably, pre-spray-dried nanocapsule dispersions did not significantly improve rainfastness or photoprotection, whereas the spray-dried hierarchical structures exhibited enhanced resistance to wash-off under rainfall conditions, improved protection against UV-induced quercetin photodegradation, and more sustained quercetin release. These findings highlight the functional importance of the engineered pomegranate-like hierarchical architecture. Furthermore, biological assays using pea seedlings (*Pisum sativum* L.) and black bean aphid (*Aphis fabae*) demonstrated effective pest deterrence and promotion of plant growth. Our delivery system represents a promising platform for dual-function agrochemical delivery.

1. Introduction

Amid increasing pressure on global agricultural production, strategies to meet food demands while maintaining environmental sustainability are receiving growing attention [1]. Synthetic pesticides play a traditional and critical role in agricultural production [2]. While they provide effective pest control, they also result in potential environmental risks, particularly the accumulation of residues in soil, toxic effects on non-target organisms, and ecosystem disruption [2–4]. These concerns have led to increasingly stringent regulations on conventional chemical pesticides and growing consumer demand for residue-free agricultural products [4,5]. Under these circumstances, biopesticides derived from natural products have emerged as an important strategy for reducing reliance on synthetic pesticides because of their rapid biodegradability, lower toxicity, and multiple pest-targeting mechanisms, including antifeedant activity, growth disruption, and metabolic interference [3,6]. Among the many natural bioactive compounds, flavonoids have attracted considerable attention as potential biopesticides due to their structural diversity and broad biological activities [6,7]. Quercetin, a flavonoid widely distributed in plants, exhibits antioxidant activity, a bitter taste, and multi-target physiological toxicity [8,9]. As an antifeedant biopesticide, quercetin differs fundamentally from conventional neurotoxic insecticides by suppressing feeding behaviour and disrupting physiological metabolism rather than inducing immediate mortality, thereby reducing selection pressure for resistance development [7,8,10]. This represents a potentially more sustainable strategy for pest management. However, practical application of quercetin remains severely constrained by its extremely poor aqueous solubility, which limits formulation into effective sprayable preparations [11,12]. Furthermore, weak foliar adhesion and rapid photodegradation under ultraviolet radiation substantially shorten its effective field persistence [11–13]. These limitations reduce delivery efficiency, bioavailability,

* Corresponding author.
E-mail address: rori0610@graduate.hku.hk (W.-F. Lai).

https://doi.org/10.1016/j.jconrel.2026.115227
Received 3 February 2026; Received in revised form 13 July 2026; Accepted 30 July 2026
Available online 31 July 2026

and pest control performance, highlighting the need for advanced delivery systems capable of protecting quercetin while enabling controlled and targeted release.

Nanotechnology-enabled encapsulation systems have recently emerged as promising platforms for improving the delivery performance of natural pesticides by enhancing stability, improving bioavailability, reducing off-target losses, and enabling controlled release [2,4,14]. Among the available carrier materials, proteins have attracted considerable interest because of their excellent biocompatibility, biodegradability, self-assembly behaviour, and capacity for controlled release [15–17]. Protein-based nanocapsules are also relatively simple to prepare and readily scalable for industrial production [18,19]. Compared with animal-derived proteins, plant proteins offer additional advantages, including lower cost, abundant agricultural availability, and greater sustainability, thereby aligning with the principles of sustainable agriculture and the circular economy [16,20–22]. Despite these advantages, most existing protein-based delivery systems have been constructed from single protein components [23,24]. Such systems generally optimise only individual performance characteristics, such as encapsulation efficiency or release behaviour, but often fail to simultaneously satisfy the multiple stability requirements encountered in agricultural environments, including ultraviolet irradiation, rainfall erosion, storage stability, and the alkaline digestive conditions of insect pests [18,25,26]. Consequently, the development of multifunctional protein-based delivery systems capable of simultaneously protecting bioactive compounds, enabling environmentally responsive release, and maintaining field stability remains an important challenge in controlled-release research. Furthermore, previous studies have focused primarily on pesticide encapsulation, release kinetics, and biological efficacy, whereas the potential agronomic functionality of carrier materials has received comparatively little attention [27,28]. Plant-derived proteins can be gradually degraded by soil microorganisms into amino acids and small peptides, thereby acting as slow-release nitrogen sources capable of promoting crop growth [18]. This suggests that protein-based delivery systems may serve not only as pesticide carriers but also as nutrient-delivery materials, offering opportunities to integrate controlled pesticide delivery with fertilisation. However, such multifunctional delivery strategies remain largely unexplored.

To address these challenges, we developed a hierarchical soy protein isolate (SPI)-zein delivery platform for encapsulating the hydrophobic flavonoid biopesticide quercetin. SPI contributes hydrophilicity, interfacial stabilisation, and film-forming capability, whereas the hydrophobic self-assembly behaviour of zein provides an effective microenvironment for encapsulating poorly water-soluble bioactive compounds [6,29–34]. Inspired by the hierarchical architecture of pomegranate fruit, in which numerous seed-like units are organised into a higher-order assembly, we designed a bioinspired multi-scale delivery system for agricultural applications [35–37]. A pomegranate-like hierarchical structure was fabricated through spray drying, during which rapid droplet solidification assembled and immobilised numerous quercetin-loaded nanocapsules within micron-sized particulate aggregates. Within this hierarchical architecture, zein-rich domains provide hydrophobic confinement that enhances quercetin stability, whereas SPI contributes environmental responsiveness and interfacial integrity. The resulting multi-scale organization simultaneously protects quercetin against environmental degradation, improves formulation stability, and enables pH-responsive release under target conditions. Beyond controlled pesticide delivery, gradual biodegradation of the protein matrix also provides a potential slow-release nutrient source for crop growth, thereby integrating pest control with plant growth promotion within a single biodegradable delivery platform. Overall, this study presents the first bioinspired hierarchical SPI-zein delivery system for quercetin that simultaneously integrates cargo protection, environmentally responsive controlled release, and agronomic nutrient functionality. More broadly, this work establishes a multifunctional biodegradable protein-based controlled-release platform that extends beyond conventional pesticide encapsulation, providing both a conceptual framework and a practical strategy for developing next-generation sustainable agricultural formulations.

Table 1
Amounts of materials used in the preparation of SPI-zein nanocapsules with different SPI:zein mass ratios.

SPI:zein mass ratio	SPI (g)	Zein (g)	Quercetin (mg)	70% (v/v) ethanol (mL)	Deionized water (mL)
1:0	6	0	50	80	120
2:1	4	2	50	80	120
1:1	3	3	50	80	120
1:2	2	4	50	80	120
0:1	0	6	50	80	120

2. Materials and methods

2.1. Materials

Zein (purity ≥20 ppm), absolute ethanol (> 99.8%), hydrochloric acid (37%) and sodium hydroxide were purchased from Fisher Scientific (Loughborough, UK). SPI was purchased from MP Biomedicals Europe (Illkirch-Graffenstaden, France). Quercetin was purchased from Fluorochem (Hadfield, UK). Black bean aphids (*Aphis fabae*) were provided by Harper Adams University (Newport, Shropshire, UK). Pea seeds and shoots (*Pisum sativum* L.) were purchased from local suppliers in the United Kingdom. Deionized water was used throughout the experiments.

2.2. Preparation of quercetin-loaded SPI-zein nanocapsules

To prepare quercetin-loaded SPI-zein nanocapsules, a predetermined amount of zein was dissolved in 70 mL of 70% (*v*/v) ethanol and magnetically stirred at 300 rpm for 1 h. In parallel, SPI was dispersed in 120 mL of deionized water at pH 7 and stirred at 300 rpm for 1 h. The amounts of SPI and zein used for nanocapsule preparation are listed in Table 1. Quercetin was dissolved at a concentration of 5 mg/mL in 10 mL of 70% (*v*/v) ethanol under light-protected conditions. The solution was stirred continuously on a magnetic stirrer (SHP-200-MP Hotplate Stirrer, Cole-Parmer, USA) at 200 rpm for 30 min at room temperature. The quercetin solution was then mixed with the zein solution to form the organic phase, which was subsequently added dropwise into the SPI aqueous solution under continuous stirring. The resulting mixture was further stirred at 300 rpm for 2 h to facilitate the formation of quercetin-loaded nanocapsules via antisolvent-induced self-assembly.

2.3. Preparation of the bioinspired delivery systems

The quercetin-loaded nanocapsule dispersions were spray-dried using a Mini Spray Dryer (B-290, Büchi Labortechnik AG, Switzerland) equipped with a twin-fluid nozzle. The spray-drying conditions were as follows: nozzle diameter, 0.7 mm; air flow rate, 357 L/h; rotameter pressure drop, 0.23 bar; feed flow rate, 6 mL/min; and inlet and outlet temperatures of 140 °C and 90 °C, respectively [38]. The total solid content of the feed dispersion was maintained at 3.0% (*w*/*v*), while different formulations were prepared by varying the SPI:zein ratio. The dispersions were kept under continuous stirring at 200 rpm throughout the spray-drying process under controlled laboratory humidity (45–55% RH). After spray drying, the resulting powder, constituting the delivery system, was collected in sealed bags and stored in a desiccator at room temperature. Delivery systems with SPI:zein mass ratios of 1:0, 2:1, 1:1, 1:2, and 0:1 were designated as QueSZ10, QueSZ21, QueSZ11, QueSZ12, and QueSZ01, respectively. Blank delivery systems without quercetin, prepared using the same SPI:zein ratios, were also generated and designated as SZ10, SZ21, SZ11, SZ12, and SZ01, respectively. The powder yield (PY) was calculated using Eq. (1), where X_{wb} is the

moisture content on a wet basis, M_V is the feed volume (L), T_S is the total solids content (g dry matter/L), and W_1 and W_2 are the weights (g) of the container before and after the spray-drying process, respectively.

$$PY\ (\%) = \frac{(W_2 - W_1) - X_{wb}(W_2 - W_1)}{M_V T_S} \quad (1)$$

2.4. Cryo-electron microscopy (cryo-EM) analysis

Cryo-EM grids (Quantifoil R 1.2/1.3 Cu 300) were glow-discharged at 15 mA for 40 s prior to use and prepared using a plunge freezer (Leica EM GP, Leica Microsystems, Germany). 3 μL of a 100-fold diluted quercetin-loaded SPI-zein nanocapsule dispersion was applied to a grid, followed by 1 μL to the reverse side. Blotting was performed for up to 5 s. Cryo-EM images were captured using an electron microscope (Titan Krios G4, Thermo Fisher Scientific, USA) equipped with a direct electron detector (Falcon 4i, Thermo Fisher Scientific, USA).

2.5. Measurement of particle size, polydispersity index (PDI), and zeta potential

Particle size, PDI, and zeta potential of the nanocapsule dispersions were measured using a Zetasizer Ultra (Malvern Panalytical, UK), equipped with a DTS0012 cuvette and operated at a 90° scattering angle.

2.6. Rheological analysis of the nanocapsule dispersions

The rheological properties of the nanocapsule dispersions were assessed using a rheometer (Modular Compact Rheometer 302, Anton Paar, Austria) with a parallel-plate geometry (25 mm diameter, 1 mm gap). Shear rheology tests were performed in controlled shear rate mode over a shear rate range of 0–300 s^{-1}. Each sample was analyzed at three temperatures (4 °C, 25 °C, and 37 °C).

2.7. Measurement of protein solubility

500 mg of the sample was dispersed in 40 mL of 0.1 M NaCl solution (pH 3.0 or 7.0) and stirred at 300 rpm for 1 h. The mixture was then adjusted to a final volume of 50 mL, followed by centrifugation at 17,800 ×*g* for 30 min. The supernatant was collected and mixed with bicinchoninic acid (BCA) reagent (2:1, *v*/v), followed by incubation at 37 °C for 30 min. Absorbance was measured at 562 nm, and protein concentration was determined using a bovine serum albumin (BSA) standard curve [39]. The calibration equation was $y = 0.08\times + 0.0037$ ($R^2 = 0.9983$). Protein solubility was calculated according to Eq. (2), where M_t is the protein mass in the supernatant, and M_0 is the total protein mass.

$$Protein\ solubility\ (\%) = \frac{M_t}{M_0} \times 100 \quad (2)$$

2.8. Measurement of moisture content

Approximately 0.3 g of the sample was placed in a pre-weighed crucible dish. The combined weight of the sample and crucible was recorded, and the sample was oven-dried at 105 °C for 4 h. Moisture content was calculated according to Eq. (3), where W_{sd} is the weight of the sample plus dish before drying (g), W_{dd} is the weight of the sample plus dish after drying (g), and W_d is the weight of the empty dish (g).

$$Moisture\ content\ (\%) = \frac{W_{sd} - W_{dd}}{W_{sd} - W_d} \times 100 \quad (3)$$

2.9. Measurement of hygroscopicity

0.5 g of the sample was placed in a desiccator containing a saturated NaCl solution, which maintained a relative humidity (RH) of 75.3% at room temperature. The samples were weighed after 24 h, 48 h, and 7 days [40]. Hygroscopicity was calculated according to Eq. (4), where W_0 is the initial dry weight of the sample (g), and W_t is the weight of the sample after equilibration under controlled relative humidity (g).

$$Hygroscopicity\ (\%) = \frac{W_t - W_0}{W_0} \times 100 \quad (4)$$

2.10. Measurement of redispersibility of the delivery systems

The delivery systems generated by spray drying were reconstituted in deionized water (1 mg/mL), followed first by vortexing (30 s) and then by probe sonication (VCX750, Sonics & Materials Inc., USA) (160 W nominal power, 20 kHz, for 2 min). The particle size was measured by DLS. The redispersibility index (RDI) was calculated according to Eq. (5) [41], where *AFD* and *BFD* indicate the particle size of the nanocapsule dispersion and that of the reconstituted delivery system, respectively.

$$RDI = \frac{AFD}{BFD} \quad (5)$$

2.11. Determination of loading capacity (LC) and encapsulation efficiency (EE)

EE and LC were determined using spectrophotometric analysis as previously described [42]. In brief, 20 mg of the quercetin-loaded spray-dried sample was weighed and dispersed in 10 mL of deionized water. The dispersion was then centrifuged (ROTINA 380R, Hettich, Germany) at 10,000 ×g for 10 min at 4 °C, and the supernatant was carefully collected for analysis. The concentration of quercetin was determined at 374 nm using a UV–Vis spectrophotometer (Model 6715, Jenway, UK). EE and LC were calculated according to Eq. (6) and Eq. (7), where C_F is the amount of quercetin in the supernatant, C_T is the total amount of quercetin added during preparation of the quercetin-loaded spray-dried sample, and C_P is the initial dry mass of the spray-dried sample used.

$$EE\ (\%) = \frac{C_T - C_F}{C_T} \times 100 \quad (6)$$

$$LC\ (\%) = \frac{C_T - C_F}{C_P} \times 100 \quad (7)$$

2.12. Scanning electron microscopy (SEM) analysis

The morphological features of the samples were imaged using SEM (Nova NanoSEM 450, FEI Company, USA) at an acceleration voltage of 15 kV. Before imaging, the spray-dried sample was placed on a double-sided conductive adhesive mounted on the sample holder and sputter-coated with gold.

2.13. Fluorescence spectroscopy analysis

Intrinsic fluorescence spectroscopy was performed using a spectrofluorometer (FluoroMax, HORIBA Scientific, Japan) with an excitation wavelength of 280 nm, an emission wavelength range of 290–450 nm, excitation and emission slit widths of 5 nm, a data acquisition interval of 1.0 nm, and a scanning speed of 600 nm/min.

2.14. Attenuated total reflectance-Fourier transform infrared (ATR-FTIR) spectral analysis

ATR-FTIR spectra were obtained using a vacuum spectrometer (Vertex 80v, Bruker, Germany) equipped with an attenuated total reflectance (ATR) accessory. The spray-dried sample was placed onto the ATR crystal, and a pressure clamp was applied to ensure optimal contact between the sample and the crystal surface. Spectra were

collected over the wavenumber range of 650–4000 cm^{-1} with a spectral resolution of 4 cm^{-1}.

2.15. UV–vis transmittance and UV-blocking analysis

The UV–Vis transmittance spectra of the spray-dried samples were measured using a UV–Vis spectrophotometer (Specord 210 Plus, Analytik Jena, Germany) over a wavelength range of 200–700 nm. The UV-blocking factor (UVBF) was calculated as the ratio of the average transmittance in the visible region (400–700 nm) to the transmittance at 350 nm [43].

2.16. X-ray diffraction (XRD) analysis

The crystalline structures of the spray-dried samples were analyzed using an X-ray diffractometer (D2 Phaser, Bruker, Germany). The XRD patterns were recorded at room temperature over a 2θ range of 5° to 80° at a scanning rate of 5°/min.

2.17. Analysis of thermal properties

Thermogravimetric analysis (TGA), derivative thermogravimetry (DTG), and differential scanning calorimetry (DSC) measurements were performed using a simultaneous thermal analyzer (SDT650, TA Instruments, USA). Approximately 5 mg of the spray-dried sample was placed in a crucible and heated from 40 °C to 600 °C at a heating rate of 10 °C/min under a nitrogen atmosphere with a flow rate of 100 mL/min.

2.18. Determination of release profiles

Quercetin release was evaluated under three pH conditions representing different agricultural environments: pH 3.5 (simulating acidic rain conditions), pH 6.8 (neutral irrigation water), and pH 8.5 (insect alkaline gut). Release studies were conducted in deionized water with pH adjusted using 0.1 M HCl or 0.1 M NaOH. 100 mg of the quercetin-loaded spray-dried sample was dispersed in 100 mL of pH-adjusted deionized water and maintained under continuous magnetic stirring at 150 rpm. At different time points, 3 mL of sample was withdrawn and immediately centrifuged at 10,000 ×*g* for 10 min. An equal volume of fresh pH-adjusted medium was added after each sampling. The absorbance of quercetin was measured at 374 nm using a UV spectrophotometer, with the percentage of cumulative release being calculated as previously reported [44]. The experimental release data were fitted using several classical kinetic models, including the zero-order, first-order, Higuchi, and Korsmeyer-Peppas models [45,46]. To determine the release mechanism, the first 80% of the cumulative release data were fitted to the Korsmeyer-Peppas model [47]. The correlation coefficients (R^2) were used to evaluate the goodness of fit and identify the predominant release mechanism.

2.19. Determination of wettability of the delivery systems on pea leaf surfaces

Fresh pea leaves were washed with deionized water and then air-dried for 30 min. Leaf sections (2 × 2 cm) were placed on glass slides with the upper leaf surface facing upwards. Using a microsyringe, 5 μL droplets of either quercetin-loaded spray-dried samples (reconstituted in deionized water at a concentration of 5 mg/mL) or deionized water (control) were deposited onto the leaf surface. Contact angle measurements were performed immediately after droplet deposition using a contact angle goniometer (OCA 25, Dataphysics, Germany).

2.20. Evaluation of retention ability of the delivery systems on pea leaf surface

Leaf sections (2 × 2 cm) were prepared. 2.5 g of the spray-dried sample was reconstituted in 50 mL of deionized water. The beaker containing the reconstituted sample, together with the tweezers, was weighed to give W_1. Leaf sections were immersed in the reconstituted sample for 10 s and then held above the beaker for 2 min to drain. The beaker and tweezers were reweighed to give W_2. Retention (R, mg/cm^2) was calculated according to Eq. (8) [2], where L_1 and L_2 are the retained volumes (mL) calculated from W_1 and W_2, respectively, assuming a density of the reconstituted sample of approximately 1000 mg/mL. C is the concentration of the reconstituted sample (mg/mL), and S is the leaf area (cm^2).

$$R = \frac{(L_1 - L_2)/1000 \times C}{S} \tag{8}$$

2.21. Evaluation of rainfastness of the delivery systems on pea leaf surface

Leaves were immersed for 1 min in either reconstituted spray-dried samples (5 mg/mL in deionized water) or quercetin-loaded SPI-zein nanocapsule dispersions, and then air-dried at room temperature for 24 h. Artificial rainfall was simulated by continuously dropping 20 mL of deionized water onto the leaf surfaces over 5 min using a pipette, while the leaves were positioned at a 45° inclination angle. After rainfall treatment, the remaining quercetin on the leaf surfaces was extracted with 70% ethanol under ultrasound for 10 min. The extracts were centrifuged at 10,000 ×*g* for 10 min, and the supernatant was then analyzed using UV–Vis spectrophotometry. Rainfastness (%) was calculated according to Eq. (9), where Q_r is the residual quercetin content after rainfall and Q_i is the initial quercetin content before rainfall.

$$\textit{Rainfastness}\ (\%) = \frac{Q_r}{Q_i} \times 100 \tag{9}$$

2.22. Evaluation of photochemical stability

Free quercetin, quercetin-loaded spray-dried samples, and quercetin-loaded nanocapsule dispersions were each dispersed in deionized water at an equivalent quercetin concentration. The samples were exposed to UV lamp irradiation (ZF-7 A, Guanghao Analytical Instruments, China) at 365 nm (16 W) with a fixed distance of 30 cm. At different time points (0, 30, 60, 90, 120, and 180 min), 3 mL of sample was withdrawn to determine the retention ratio (Eq. (10)). The photodegradation rate constant (k) and half-life ($t_{1/2}$) were calculated using Eqs. (11)–(12) [41], where C_t and C_0 are the concentrations of quercetin at time t and at the initial time, respectively.

$$\textit{Retention ratio} = \frac{C_t}{C_0} \tag{10}$$

$$ln\left(\frac{C_t}{C_0}\right) = -kt \tag{11}$$

$$t_{1/2} = \frac{ln2}{k} \tag{12}$$

2.23. Storage stability of the quercetin-loaded delivery systems

2 g of the quercetin-loaded spray-dried samples were stored in glass bottles at 25 °C and 60% relative humidity. All samples were analyzed for moisture content and quercetin retention at 0, 30, 60, and 90 days. The quercetin retention ratio was calculated according to Eq. (10). The flowability of the spray-dried samples was evaluated by measuring the angle of repose using the fixed funnel method [48]. A funnel (stem diameter = 10 mm) was mounted vertically 10 cm above a flat surface. Approximately 10 g of each sample was added to the funnel and allowed to flow freely to form a conical heap. The angle of repose (θ) was calculated according to Eq. (13), where h is the height of the cone (cm)

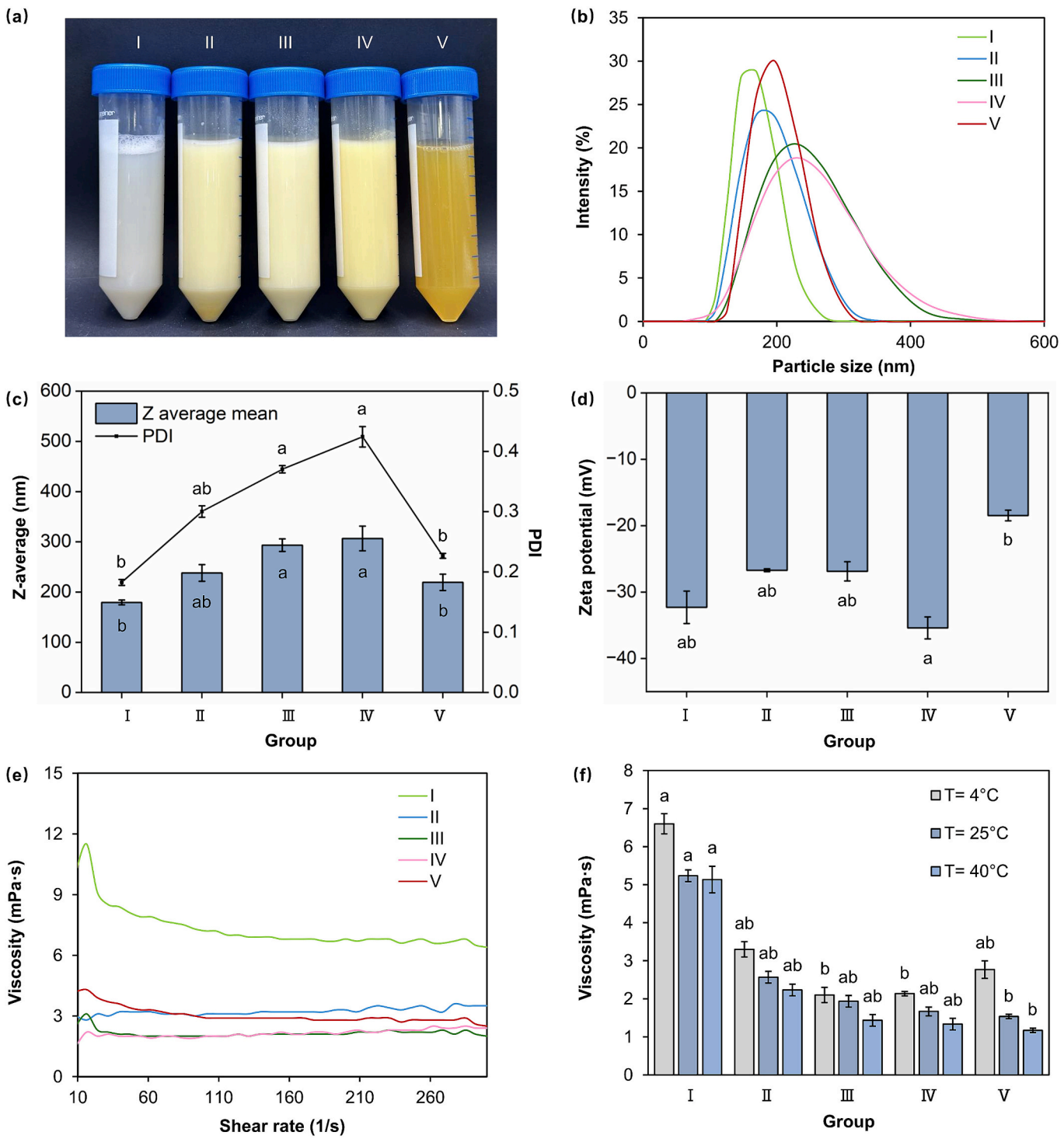

Fig. 1. Characterisation of the nanocapsule dispersions prior to spray drying. (a) Photographs of the nanocapsules. (b) Particle size distribution profiles. (c) *Z*-average diameter (bars) and PDI values (line). (d) Zeta potential values. (e) *V*iscosity as a function of shear rate at 25 °C. (f) Temperature-dependent viscosity profiles at 4, 25, and 40 °C. Roman numerals (I-V) correspond to nanocapsules with SPI:zein mass ratios of 1:0, 2:1, 1:1, 1:2, and 0:1, respectively.

and r is the radius of the base (cm).

$$tan\theta\,(^{\circ}) = \frac{h}{r} \tag{13}$$

Color stability was measured using a colorimeter (CM-700d, Konica Minolta, Japan). The spray-dried samples were placed in Petri dishes and measured at three random positions. Color parameters, including lightness (L^*), redness-greenness (a^*), and yellowness-blueness (b^*), were recorded, and the total color difference (ΔE^*) was calculated according to Eq. (14). Photographs of the samples were also taken at different time points under standardized lighting conditions.

$$\Delta E^* = \sqrt{(\Delta L^*)^2 + (\Delta a^*)^2 + (\Delta b^*)^2} \tag{14}$$

2.24. Feeding deterrence assay and long-term mortality of aphids

Quercetin-loaded spray-dried samples were dispersed in deionized

Table 2
Physicochemical characteristics of the quercetin-loaded SPI-zein delivery systems.

System	Hygroscopicity (g/100 g)	Moisture content (% *w*/w)	Protein solubility (%)	RDI	EE (%)	LC (%)	PY (%)
QueSZ10	15.47 ± 0.81 ^{a}	7.87 ± 0.64 ^{a}	76.58 ± 0.38 ^{a}	1.70 ± 0.14 ^{b}	65.3 ± 1.45 ^{b}	1.75 ± 0.04 ^{c}	60.56 ± 6.18 ^{a}
QueSZ21	11.60 ± 0.69 ^{ab}	5.60 ± 0.72 ^{ab}	65.79 ± 1.00 ^{ab}	2.87 ± 0.20 ^{ab}	72.8 ± 1.61 ^{ab}	2.27 ± 0.08 ^{bc}	45.83 ± 4.68 ^{b}
QueSZ11	11.13 ± 0.76 ^{abc}	5.33 ± 0.42 ^{ab}	51.95 ± 0.71 ^{abc}	2.64 ± 0.34 ^{ab}	78.6 ± 1.84 ^{a}	2.76 ± 0.08 ^{abc}	45.28 ± 2.87 ^{b}
QueSZ12	7.80 ± 0.80 ^{bc}	4.33 ± 0.31 ^{b}	42.04 ± 0.94 ^{bc}	3.18 ± 0.64 ^{ab}	75.2 ± 1.51 ^{ab}	3.23 ± 0.11 ^{a}	51.22 ± 2.87 ^{ab}
QueSZ01	6.73 ± 0.76 ^{c}	3.40 ± 0.35 ^{b}	22.04 ± 0.33 ^{c}	5.63 ± 1.92 ^{a}	72.3 ± 2.79 ^{ab}	2.90 ± 0.05 ^{ab}	43.72 ± 4.02 ^{ab}

water to obtain final quercetin concentrations of 10, 50, and 100 μg/mL. Free quercetin solutions were prepared at the same quercetin concentrations to match the quercetin content of the loaded samples. For the blank carrier control, a dispersion of the SZ12 formulation was prepared based on the same protein solid content that matched the quercetin-loaded delivery system. The antifeedant bioassays were conducted as previously reported [49]. In brief, fresh pea shoots were immersed in the dispersions for 10 s and air-dried for 30 min, then placed into Petri dishes. Healthy apterous adult black bean aphids were selected and starved for 2 h prior to the experiment. After starvation, 10 aphids were transferred to each dish. Dishes were maintained at 24 ± 1 °C and 60 ± 5% relative humidity. The assays lasted 8 h, and feeding aphids were counted at 1, 4, and 8 h. Aphids were considered feeding when they remained stationary on a shoot for more than 30 s. Each treatment was performed in three independent biological replicates, with a fresh batch of aphids used for each replicate (10 aphids per dish). The antifeedant ratio (AR) was calculated according to Eq. (15), where N_c and N_t represent the numbers of aphids on untreated and treated shoots, respectively, at each time point.

$$AR\ (\%) = \left(\frac{N_c - N_t}{N_c + N_t}\right) \times 100\% \tag{15}$$

Leaves were treated with the dispersions prepared above at a quercetin concentration of 50 μg/mL. They were then air-dried. Ten aphids were placed on each treated leaf and maintained under controlled environmental conditions (20 °C, 60% relative humidity). Mortality was recorded over a 12-day period. Each treatment was performed in triplicate for each formulation. Survival (%) was calculated according to Eq. (16), where N_0 is the initial number of aphids and N_t is the number of surviving aphids at time t.

$$Survival\ (\%) = \left(\frac{N_t}{N_0}\right) \times 100 \tag{16}$$

2.25. Biological evaluation in a pea growth model

The quercetin-loaded spray-dried samples were incorporated into soil at 250 mg/kg (dry weight basis). Free quercetin was added to soil at around 7.5 mg/kg (dry weight basis), corresponding to the equivalent quercetin content present in the soil treated with the quercetin-loaded spray-dried samples (based on the LC around 3%). Plain SPI-zein spray-dried samples were mixed into soil at 242.5 mg/kg (dry weight basis) as a carrier control. Untreated soil served as the blank control. Pre-germinated seedlings were transplanted into individual pots (8 cm diameter) containing 200 g of treated soil and transferred to a controlled-environment chamber for cultivation at 22 ± 2 °C (day) and 18 ± 2 °C (night) under a 16:8 h photoperiod. Plants were irrigated with deionized water every 2 days without additional fertilizer. Growth parameters, including plant height, leaf width, fresh weight, and dry weight, were measured at 3, 7, and 14 days.

2.26. Statistical analysis

All results are presented as mean ± standard deviation based on three independent experiments. Statistical analyses were performed using the Kruskal-Wallis test, followed by Dunn's multiple comparisons test with the Benjamini-Hochberg correction. Different lowercase letters indicate statistically significant differences ($p < 0.05$).

3. Results and discussion

3.1. Formation and characterisation of the nanocapsule dispersions

The bioinspired pomegranate-like delivery system was designed based on the contrasting interfacial properties of SPI and zein to form nanocapsules with a putative core-shell structure, which were subsequently assembled into microparticles via spray-drying. Based on the properties of SPI and zein, the formation process is expected to involve hydrophobic self-assembly of zein during the antisolvent process, induced by solvent exchange from ethanol to water. Hydrophilic SPI molecules then adsorb onto zein-rich nanodomains, stabilising nanocapsules with a putative core-shell structure in colloidal dispersion. During spray-drying, multiple nanocapsules are encapsulated within individual droplets, giving rise to the bioinspired pomegranate-like architecture. To support this structural hypothesis, Cryo-EM was used to observe the nanocapsules (Fig. S1). Compared with pure zein nanocapsules, SPI-zein nanocapsules exhibited a lighter outer region surrounding a darker core, suggesting the presence of an SPI-enriched shell surrounding zein-rich domains.

The properties of the nanocapsules were characterised prior to spray drying (Fig. 1a). Nanocapsules prepared with different SPI:zein mass ratios exhibited a single peak in the particle size distribution, indicating good colloidal uniformity (Fig. 1b). Among the formulations, nanocapsules prepared with SPI alone showed the smallest average particle size (~179 nm), whereas those prepared with zein alone exhibited a larger size (~219 nm). For SPI-zein nanocapsules, particle size initially increased but then decreased with increasing SPI content, ranging from ~306 nm at an SPI:zein ratio of 1:2 to ~238 nm at 2:1. This trend suggests that SPI likely contributes to the suppression of zein aggregation, resulting in smaller and more uniform nanocapsules. This effect is partly attributed to the fact that zein is highly hydrophobic and prone to self-aggregation [50], whereas SPI contains more hydrophilic functional groups and exhibits greater molecular flexibility [51]. Consequently, SPI can adsorb onto zein-rich regions, providing steric stabilisation and electrostatic repulsion that inhibit aggregation, thereby reducing particle size [52]. Finally, the PDI values ranged from 0.18 to 0.42 across all formulations (Fig. 1c), indicating acceptable size distribution and colloidal stability. Zeta potential analysis further revealed that all nanocapsules carried a negative surface charge (Fig. 1d). The most negative value (−35.4 mV) was observed for nanocapsules at an SPI:zein ratio of 1:2, suggesting that lower SPI content increased the magnitude of the negative surface charge. As SPI content increased, the absolute zeta potential decreased moderately to approximately −26 mV for nanocapsules at SPI:zein ratios of 1:1 and 2:1.

The rheological properties of the nanocapsule dispersions are important for subsequent spray-drying performance. All dispersions exhibited shear-thinning behaviour (Fig. 1e). The dispersion prepared using SPI alone showed the highest viscosity (~6.5 mPa·s), whereas dispersions containing both SPI and zein exhibited lower viscosities (2.0–3.5 mPa·s). Temperature-dependent measurements at 4, 25, and 40 °C further showed that the viscosity of all dispersions decreased with increasing temperature (Fig. 1f). The viscosity of the SPI-only dispersion decreased from ~6.5 to ~5.0 mPa·s as the temperature increased from 4

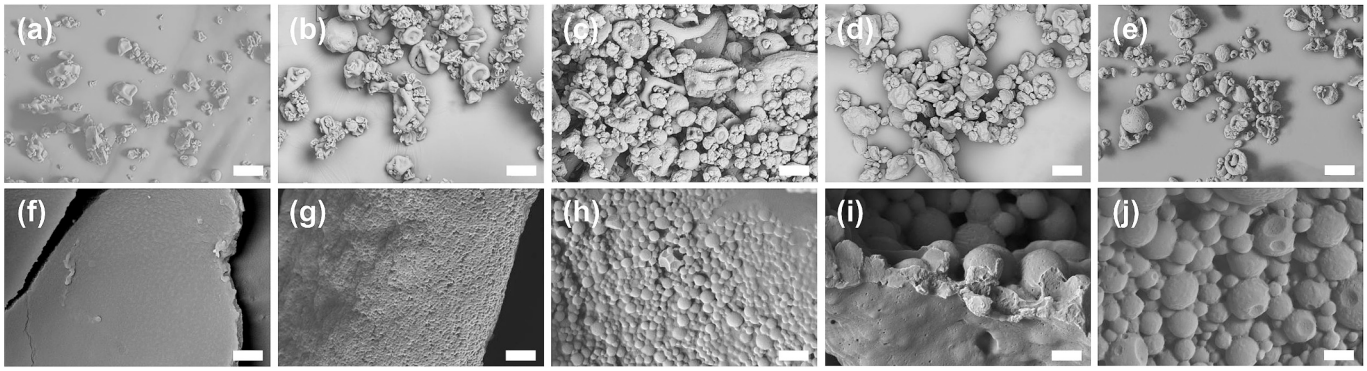

Fig. 2. SEM micrographs of quercetin-loaded SPI-zein delivery systems. The images were captured at (a-e) 500× and (f-j) 20,000× magnifications for different formulations: (a, f) QueSZ10, (b, g) QueSZ21, (c, h) QueSZ11, (d, i) QueSZ12, and (e, j) QueSZ01. Scale bars: 5 μm (a-e) and 0.2 μm (f-j).

to 40 °C. In contrast, the SPI-zein dispersions maintained relatively stable viscosities within the range of 2.0–3.5 mPa·s.

3.2. Physicochemical properties of the quercetin-loaded delivery systems

The physicochemical characteristics of the quercetin-loaded delivery systems are summarized in Table 2. Hygroscopicity decreased with increasing zein content. Based on the classification reported previously [53], hygroscopicity can generally be divided into non-hygroscopic (<10%), slightly hygroscopic (10–15%), and hygroscopic (15–20%). QueSZ10 exhibited a hygroscopicity of 15.47 ± 0.81 g/100 g and was classified as slightly hygroscopic, whereas QueSZ01 showed a much lower value of 6.73 ± 0.76 g/100 g, corresponding to the non-hygroscopic category. These results indicate that zein-rich delivery systems possess improved moisture resistance, likely due to the hydrophobic nature and relatively compact structure of zein. Previous studies have similarly reported that zein can effectively restrict water vapor permeation within protein matrices [54,55].

Moisture content measurements showed a similar trend. SPI-rich delivery systems retained higher moisture levels (7.87 ± 0.64%), whereas zein-rich ones maintained lower moisture contents (3.40 ± 0.35%). Protein solubility, an indicator related to water dispersibility and redispersion behaviour, decreased significantly with increasing zein content, dropping from 76.58 ± 0.38% to 22.04 ± 0.33%. These results suggest that increasing zein content alters the hydration and dispersion behaviour of the systems, consistent with previous reports on

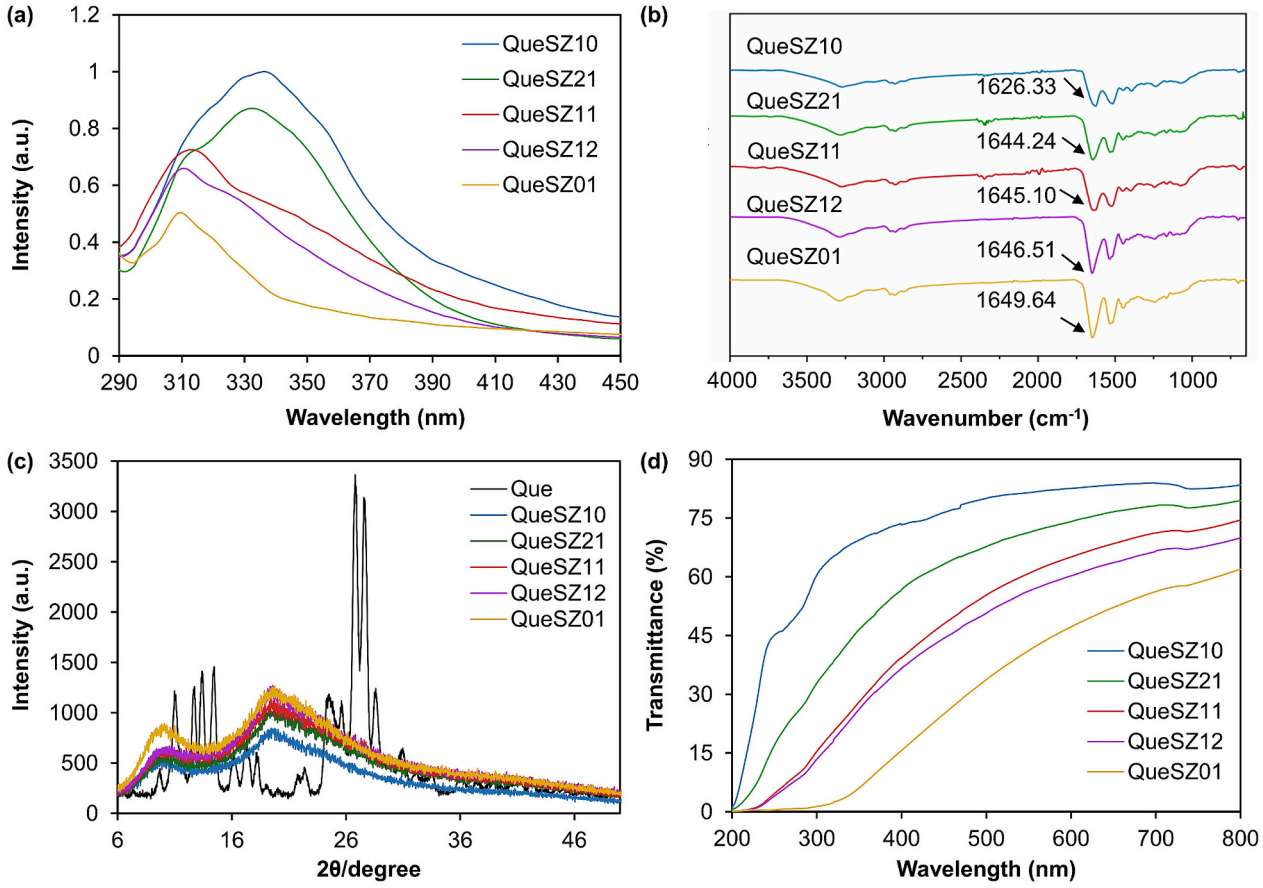

Fig. 3. Structural and molecular interaction characterisation of the quercetin-loaded SPI-zein delivery systems. (a) Intrinsic fluorescence emission spectra (excitation at 280 nm), (b) ATR-FTIR spectra, (c) XRD profiles, and (d) UV–vis transmittance spectra of the quercetin-loaded SPI-zein delivery systems.

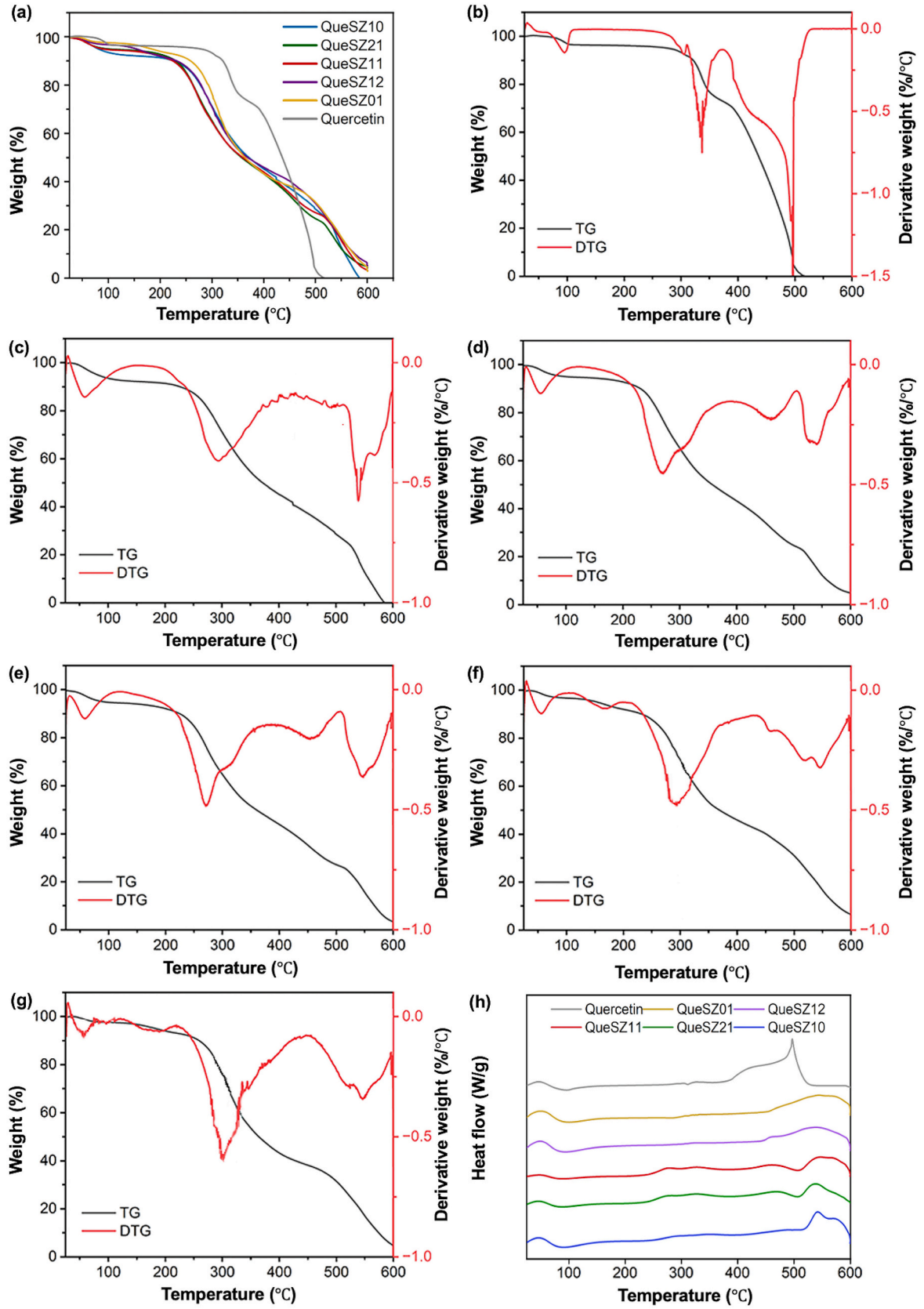

Fig. 4. Thermal analysis of the quercetin-loaded SPI-zein delivery systems. (a) TGA thermograms, along with DTG curves of (b) QueSZ10, (c) QueSZ21, (d) QueSZ11, (e) QueSZ12, (f) QueSZ01, and (g) free quercetin. (h) DSC thermograms of the delivery systems with different SPI-zein mass ratios.

hydrophobic protein-based carriers [56,57]. Redispersibility analysis further reflected differences in post-drying structural reorganization. The zein-only delivery system exhibited the highest RDI value (5.63 ± 1.92), whereas QueSZ10 showed the lowest value. In mixed SPI-zein formulations, particle size changes after redispersion were smaller, with RDI values ranging from 2.64 ± 0.34 to 3.18 ± 0.64. Moreover, increasing SPI content was associated with lower RDI values, indicating reduced particle size change upon reconstitution. Similar observations have been reported previously, where hydrophobic zein-based nanocapsules tended to form stronger inter-particle aggregates after drying, while incorporation of hydrophilic stabilisers modified their redispersion behaviour [41].

Among the delivery systems tested, QueSZ11 and QueSZ12 exhibited the highest EE, at 78.6 ± 1.84% and 75.2 ± 1.51%, respectively. Overall, the EE values (65–79%) indicate that the SPI-zein delivery systems possessed good capacity for encapsulating quercetin, although some non-encapsulated quercetin likely remained. Similar EE ranges have also been reported in other plant protein-based encapsulation systems [58,59]. In addition, LC increased progressively with increasing zein content, from 1.75 ± 0.04% for QueSZ10 to 3.23 ± 0.11% for QueSZ12. In contrast, PY decreased with increasing zein content. QueSZ10 achieved the highest yield (60.56 ± 6.18%), whereas QueSZ01 showed the lowest value (43.72 ± 4.02%). This reduction may be associated with differences in spray-drying behaviour and increased material deposition within the spray dryer during processing [58,60].

3.3. Morphology of the quercetin-loaded SPI-zein delivery systems

The morphology of the quercetin-loaded delivery systems was characterised by SEM at 500× (Fig. 2a-e) and 20,000× magnifications (Fig. 2f-j). At low magnification, all samples exhibited irregularly shaped and partially aggregated particles. The extent of aggregation and surface roughness varied with the composition of the wall materials. SPI-rich samples (QueSZ10 and QueSZ11) showed more collapsed and irregular structures, whereas zein-rich formulations (QueSZ12 and QueSZ01) exhibited more spherical and discrete particles. At higher magnification, differences in surface morphology and structural features became more evident. With increasing zein content, the particle surfaces appeared smoother and more compact [51]. In addition, variations in internal microstructural features within the spray-dried particles were observed across formulations, indicating differences in the organization of nanocapsule assemblies. These observations are consistent with the proposed formation mechanism described earlier, in which nanocapsules are formed in the colloidal dispersion prior to spray-drying [61,62]. During spray-drying, these pre-formed nanocapsules are incorporated into individual droplets, leading to the formation of micron-sized particles upon solvent evaporation [63]. This process results in a hierarchical pomegranate-like structure, where each spray-dried particle contains multiple nanocapsule assemblies resembling pomegranate seeds. The formation of this architecture is driven by rapid solvent evaporation and steep temperature gradients during spray drying, which may induce interfacial rearrangement and internal structural evolution of the droplets [61].

3.4. Structural and molecular interaction analysis of the quercetin-loaded SPI-zein delivery systems

The structural and molecular interactions within the quercetin-loaded SPI-zein delivery systems were investigated using fluorescence spectroscopy, FTIR, UV–vis spectroscopy, and XRD (Fig. 3a-d). The intrinsic fluorescence spectra revealed that QueSZ10 exhibited the highest fluorescence intensity and an emission maximum at 336 nm (Fig. 3a). The intrinsic fluorescence of tryptophan (Trp) is widely used to characterise protein conformational changes and protein-protein interactions due to its sensitivity to changes in microenvironment polarity [32]. Compared with zein-containing formulations, QueSZ10 exhibited the highest emission maximum, suggesting that Trp residues in this system experience a more polar microenvironment and less hydrophobic association [64]. As the proportion of zein increased, a blue shift in the emission maximum from 332 nm (QueSZ21) to 311 nm (QueSZ01) was observed, indicating that Trp residues are located in a more hydrophobic microenvironment. This suggests enhanced hydrophobic interactions and protein association within the SPI-zein systems [65]. The decrease in fluorescence intensity may be attributed to quercetin-induced quenching of Trp fluorescence [31], as well as the reduced contribution of Trp residues in zein [30].

The FTIR spectra of all formulations showed characteristic protein absorption bands, including O-H/N-H stretching (~3300 cm^{-1}), amide I (1626–1650 cm^{-1}), and amide II (1516–1536 cm^{-1}) (Fig. 3b). Notably, characteristic absorption peaks of crystalline quercetin were absent or significantly attenuated in all delivery systems, suggesting that quercetin may have been well incorporated within the protein matrix [66]. With increasing zein content, slight shifts in the O-H/N-H stretching band (from 3276.0 to 3285.8 cm^{-1}) were observed, reflecting changes in hydrogen-bonding environments, likely due to reduced hydration and enhanced hydrophobic interactions [67]. Concurrent shifts in amide I and amide II bands further indicate alterations in protein secondary structure and intermolecular interactions. Overall, these spectral changes support the formation of non-covalent interactions, including hydrogen bonding and hydrophobic associations, within the SPI-zein-quercetin systems, consistent with previous studies on protein-polyphenol complexes [32,68,69].

The solid-state organization of the delivery systems was further investigated using XRD (Fig. 3c). Free quercetin exhibited sharp diffraction peaks, confirming its crystalline nature [70]. In contrast, all SPI-zein delivery systems displayed broad peaks at approximately 10° and 20°, characteristic of amorphous protein matrices, while the characteristic crystalline peaks of quercetin were absent [52]. With increasing zein content, the intensity of these broad peaks increased, suggesting tighter molecular packing and enhanced short-range ordering, likely associated with stronger hydrophobic interactions in zein-rich matrices. In contrast, SPI-rich formulations exhibited broader and weaker diffraction features, indicating a less compact molecular arrangement. Together with the FTIR results described above, these findings suggest that quercetin was incorporated into an amorphous protein matrix, with composition-dependent internal packing influenced by the SPI-zein ratio.

In UV–vis spectra, all formulations exhibited good transparency in the visible range (400–700 nm), with transmittance values of approximately 45–80% (Fig. 3d). Increasing zein content led to reduced visible light transmittance. In the UV region (280–400 nm), all systems showed effective UV attenuation. Absorption in the UVB region (280–310 nm) is mainly attributed to aromatic amino acid residues, whereas UVA absorption (310–400 nm) is associated with π-π conjugation of encapsulated quercetin [69]. In addition, light scattering from colloidal dispersions formed upon reconstitution of the delivery systems may also contribute to the overall UV-blocking performance [71]. In particular, at higher zein contents, increased structural compactness and optical heterogeneity may enhance scattering effects due to refractive index differences between the dispersed particles and the surrounding medium. The UV-blocking factor (UVBF) ranged from 1.48 to 2.22 for the SPI-zein formulations (QueSZ21, QueSZ11, and QueSZ12), compared with 1.12 for QueSZ10 and 6.31 for QueSZ01 (Fig. S2).

3.5. Thermal analysis of the quercetin-loaded SPI-zein delivery systems

TGA and DTG analyses were performed to evaluate the thermal stability of the delivery systems. The TGA thermograms (Fig. 4a) and corresponding DTG curves (Fig. 4b-g) illustrate the thermal decomposition behaviour and associated weight-loss profiles. The initial weight loss (8–12%) below 120 °C was attributed to moisture evaporation, while the major decomposition stage associated with protein

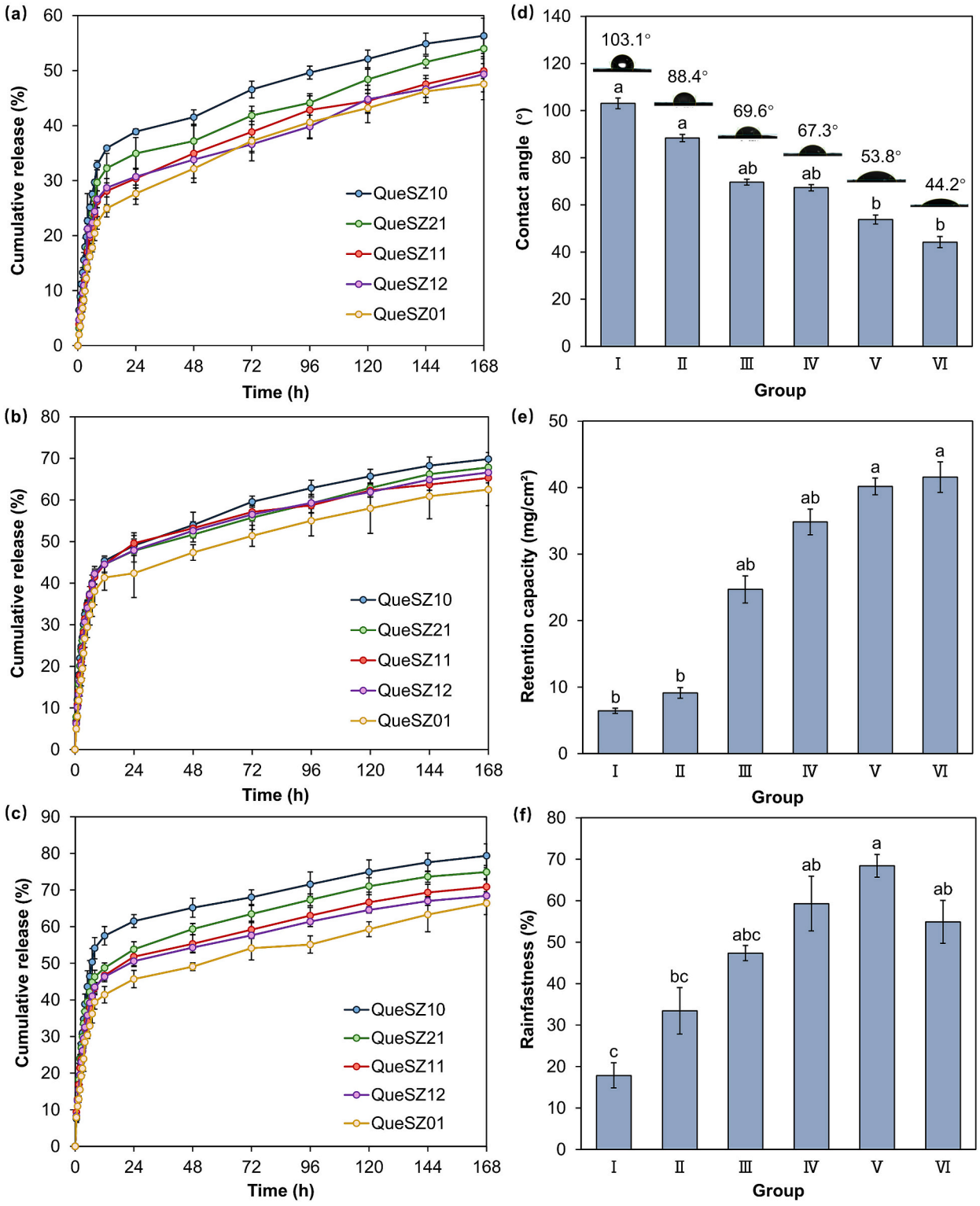

Fig. 5. Release behaviour and foliar application performance of the quercetin-loaded SPI-zein delivery systems under simulated agricultural conditions. Release profiles of quercetin from different delivery systems under (a) acidic conditions (pH 3.5), (b) neutral conditions (pH 6.8), and (c) alkaline conditions (pH 8.5). (d) Contact angle, (e) foliar retention, and (f) rainfastness of the quercetin-loaded SPI-zein delivery systems on pea leaves. Roman numerals (I-VI) in (d) and (e) correspond to water, QueSZ10, QueSZ21, QueSZ11, QueSZ12, and QueSZ01, respectively, whereas those in (f) correspond to quercetin, QueSZ10, QueSZ21, QueSZ11, QueSZ12, and QueSZ01.

degradation occurred between 280 and 350 °C [72]. The DTG profiles further revealed a gradual shift in the maximum decomposition temperature toward higher temperatures with increasing zein content, from approximately 270 °C for QueSZ10 to 300 °C for QueSZ01. This trend may be attributed to the stronger hydrophobic interactions and more compact molecular organization of zein-rich systems, which require higher thermal energy to initiate thermal degradation [50]. DSC analysis showed that all delivery systems exhibited a broad endothermic

Table 3
Kinetic parameters of release under different pH conditions.

pH		Zero-order model		First-order model		Higuchi model		Korsmeyer-Peppas model	
		k_0	R^2	k_1	R^2	k_H	R^2	n	R^2
3.5	QueSZ10	0.271	0.712	0.141	0.952	3.878	0.866	0.267	0.948
	QueSZ21	0.274	0.732	0.114	0.952	3.879	0.874	0.309	0.930
	QueSZ11	0.254	0.756	0.111	0.946	3.588	0.896	0.309	0.948
	QueSZ12	0.239	0.742	0.130	0.931	3.377	0.878	0.288	0.940
	QueSZ01	0.258	0.797	0.0880	0.948	3.608	0.927	0.346	0.961
6.8	QueSZ10	0.318	0.674	0.173	0.943	4.595	0.836	0.239	0.945
	QueSZ21	0.305	0.668	0.176	0.946	4.401	0.827	0.238	0.937
	QueSZ11	0.299	0.629	0.170	0.969	4.378	0.801	0.240	0.918
	QueSZ12	0.308	0.643	0.165	0.964	4.479	0.809	0.247	0.917
	QueSZ01	0.300	0.678	0.148	0.958	4.312	0.837	0.265	0.925
8.5	QueSZ10	0.242	0.215	0.410	0.987	4.098	0.368	0.125	0.677
	QueSZ21	0.306	0.342	0.281	0.991	4.888	0.520	0.169	0.749
	QueSZ11	0.228	0.264	0.366	0.987	3.753	0.428	0.139	0.709
	QueSZ12	0.219	0.243	0.362	0.983	3.642	0.402	0.138	0.680
	QueSZ01	0.283	0.583	0.191	0.975	4.204	0.766	0.219	0.911

transition within the range of 50–150 °C (Fig. 4h), corresponding to the evaporation of free and bound water, consistent with the initial weight-loss stage observed in TGA analysis. In addition, free quercetin exhibited a sharp endothermic peak at approximately 316 °C, corresponding to the melting of crystalline quercetin [73]. This peak was absent in all SPI-zein delivery systems, suggesting that quercetin was incorporated into the protein matrix in a non-crystalline or amorphous form, consistent with the FTIR and XRD results.

3.6. Controlled release behaviour of the quercetin-loaded SPI-zein delivery systems

The quercetin-loaded SPI-zein delivery systems exhibited pH-dependent release profiles under three agriculturally relevant pH conditions (Fig. 5a-c). All formulations displayed an initial burst release within the first 12 h, followed by a sustained release phase. Increasing zein content reduced quercetin release, which may reflect the role of the hydrophobic zein-rich matrix in restricting water penetration and thereby slowing diffusion of encapsulated quercetin [74,75]. The release behaviour was also influenced by pH. The slowest cumulative release was observed at pH 3.5 (45–55% at 168 h), whereas the highest release occurred at pH 8.5 (66–79% at 168 h). Such pH-dependent release behaviour is relevant to agricultural environments. Slower release under acidic conditions (pH 3.5, simulating acidic rainfall) could help improve retention of active compounds on leaf surfaces, whereas accelerated release at pH 8.5 is consistent with the alkaline gut conditions of many phytophagous insects, which may favor enhanced quercetin release following ingestion [76]. Here, it is worth noting that, compared with the corresponding pre-spray-dried quercetin-loaded nanocapsule dispersions, the reconstituted spray-dried SPI-zein delivery systems exhibited slower quercetin release under all tested pH conditions (Fig. S3). This behaviour is likely attributable to the pomegranate-like hierarchical architecture generated during spray drying. In these structures, multiple nanocapsules are assembled and immobilised within larger particulate aggregates, potentially creating additional diffusion barriers and more tortuous mass-transfer pathways [77,78]. Consequently, this may contribute to the retarded quercetin diffusion from the delivery systems into the release medium relative to the nanocapsule dispersions.

The release profiles were fitted using zero-order, first-order, Higuchi, and Korsmeyer-Peppas models (Table 3). Based on the R^2 values, the first-order model provided comparatively better fits ($R^2 \approx 0.931$–0.997), which may suggest that release behaviour was more closely related to the amount of quercetin remaining within the matrix than to a constant release rate. The Korsmeyer-Peppas model was further applied to evaluate the release mechanism. The n values ranged from 0.125 to 0.346 across all formulations and pH conditions, with all values below 0.45, suggesting that molecular diffusion through the protein matrix was the primary release mechanism [45]. Under alkaline conditions (pH 8.5), higher k values were observed in the first-order model, indicating accelerated release kinetics, while the Korsmeyer-Peppas model showed relatively lower fitting quality, as reflected by lower R^2 values. This reduced fit might indicate that release behaviour under alkaline conditions is not fully described by simple Fickian diffusion and may involve additional transport processes.

3.7. Foliar adhesion of the quercetin-loaded SPI-zein delivery systems

The reconstituted quercetin-loaded SPI-zein delivery systems exhibited improved wettability on leaf surfaces and increased retention compared with water (Fig. 5d-e). Water exhibited poor spreading, with a contact angle of approximately 103°, whereas QueSZ10 moderately reduced the contact angle to 88.4°, attributable to its hydrophilic nature and film-forming properties. Incorporation of zein into the formulations further modified droplet behaviour and enhanced spreading, with QueSZ12 showing a contact angle of 53.8°, corresponding to approximately a 50% reduction relative to water. Improved wettability was accompanied by a substantial increase in foliar retention, rising from 6.4 mg/cm^2 (water) and 9.1 mg/cm^2 (QueSZ10) to 24.7–41.6 mg/cm^2 for QueSZ21, QueSZ11, QueSZ12 and QueSZ01. Although zein is intrinsically more hydrophobic than SPI, the reduced contact angle is unlikely to arise from hydrophobicity alone. Instead, the SPI-zein composite particles may exhibit altered interfacial behaviour, promoting droplet spreading on the wax-rich leaf surface. Furthermore, the spray-dried particulate architecture may facilitate particle-leaf interactions after reconstitution, thereby increasing the effective contact area and improving wettability [79,80]. To further evaluate adhesion under simulated rainfall conditions, rainfastness tests were performed (Fig. 5f and Fig. S4). The rainfastness of all pre-spray-dried quercetin-loaded SPI-zein nanocapsule dispersions was not statistically different from that of free quercetin, suggesting that formulation into nanocapsule dispersions alone did not significantly improve rainfastness. However, after engineering into SPI-zein delivery systems with pomegranate-like hierarchical structures via spray drying, the formulations exhibited significantly enhanced rainfastness compared with free quercetin. This improvement is likely associated with the formation of structurally integrated particulate aggregates during spray drying, which not only enhances deposition stability but also creates more intimate particle-leaf contact after reconstitution, thereby reducing wash-off of quercetin from leaf surfaces under rainfall conditions [79,80]. Among the different formulations, QueSZ11 and QueSZ12 retained 59.3% and 68.4% of quercetin, respectively, significantly higher than free quercetin (17.86%) after washing. These results indicate that the spray-dried hierarchical SPI-zein delivery systems improve foliar retention and

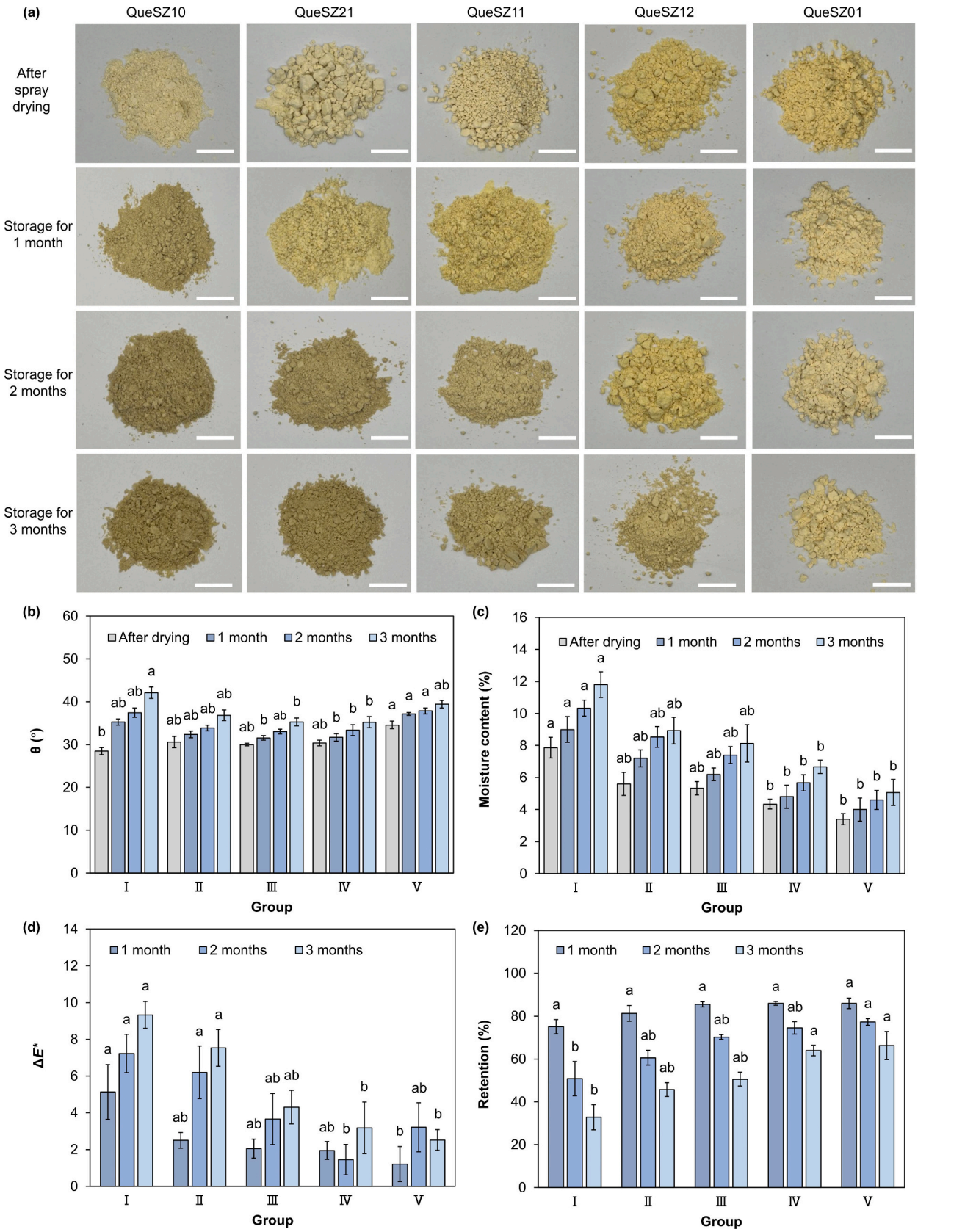

Fig. 6. Storage stability of the quercetin-loaded SPI-zein delivery systems over 3 months at 25 °C and 60% relative humidity. (a) Images of the samples at 0, 1, 2, and 3 months (scale bar = 1 cm). Changes in (b) angle of repose (θ), (c) moisture content, (d) total color difference (ΔE^*), and (e) quercetin retention ratios of the delivery systems during storage. Roman numerals (I-*V*) correspond to QueSZ10, QueSZ21, QueSZ11, QueSZ12, and QueSZ01, respectively.

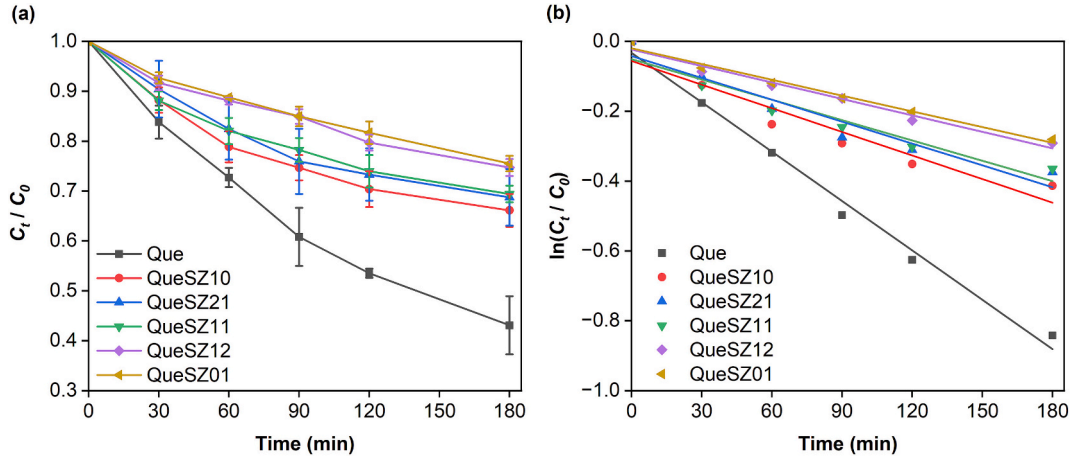

Fig. 7. Photostability of the quercetin-loaded SPI-zein delivery systems under UV irradiation. (a) Retention ratios and (b) degradation kinetics of free quercetin and that encapsulated within the delivery systems under UV exposure.

resistance to wash-off under rainfall conditions.

3.8. Storage stability of the quercetin-loaded SPI-zein delivery systems

The storage behaviour of the quercetin-loaded SPI-zein delivery systems was monitored for 3 months at 25 °C and 60% relative humidity. Systems with increasing zein content exhibited a lower rate of moisture uptake over time, resulting in a reduced angle of repose and improved flowability (Fig. 6b, c). Colorimetric analysis also revealed formulation-dependent color changes (Fig. 6a, d and Fig. S5). QueSZ10 exhibited the greatest total color difference ($\Delta E^* = 9.3$), whereas QueSZ12 ($\Delta E^* = 3.2$) and QueSZ01 ($\Delta E^* = 2.5$) remained below the commonly accepted visual threshold ($\Delta E^* < 5$). It should be noted that color change alone is not a reliable indicator of quercetin stability, as darkening in SPI-rich systems may also arise from protein-related browning reactions [81]. Regarding the changes in moisture content and color of the systems during storage, which may reflect formulation stability, the retention of encapsulated quercetin was further evaluated (Fig. 6e). The quercetin retention ratios of QueSZ12 and QueSZ01 were 0.64 ± 0.02 and 0.66 ± 0.07, respectively, whereas that of QueSZ10 was only 0.33 ± 0.06. These results suggest that higher zein content improves long-term quercetin stability, possibly due to enhanced hydrophobic shielding and reduced oxygen permeability within the matrix [82].

3.9. Photostability of the quercetin-loaded SPI-zein delivery systems

The photostability of free quercetin and that encapsulated within the delivery systems was evaluated by analysing retention ratios and degradation kinetics under UV irradiation (Fig. 7). Quercetin retention ratios for both free quercetin and quercetin encapsulated within the SPI-zein delivery systems decreased progressively during 180 min of UV irradiation. However, free quercetin exhibited a substantially greater reduction, resulting in a final retention ratio of 0.43 ± 0.06. In contrast, the retention ratios of quercetin encapsulated within the delivery systems remained within the range of 0.66–0.76. At 180 min, the quercetin retention ratios of QueSZ11, QueSZ12, and QueSZ01 were statistically significantly higher than that of free quercetin (Fig. S6a). On the other hand, quercetin encapsulated within the corresponding pre-spray-dried nanocapsule dispersions did not exhibit statistically significant differences in retention ratio compared with free quercetin after 180 min of UV irradiation, regardless of the SPI-zein mass ratio (Fig. S6b). This indicates that encapsulation within nanocapsules alone was insufficient to produce a statistically detectable improvement in photostability. In contrast, significantly higher quercetin retention than free quercetin was observed for several spray-dried delivery systems, suggesting that the pomegranate-like hierarchical particulate architecture generated through spray drying may contribute to enhanced photoprotection. Such an effect may arise from increased physical shielding of encapsulated quercetin within the pomegranate-like aggregates, thereby reducing its exposure to UV radiation [83,84].

Table 4
Half-life ($t_{1/2}$) values, photodegradation rate constant (k) and correlation coefficient (R^2) of free quercetin and quercetin encapsulated within different delivery system under UV irradiation.

Group	$t_{1/2}$/min	k	R^2
Que	147.26	0.0047	0.989
QueSZ10	300.91	0.0023	0.920
QueSZ21	329.57	0.0021	0.932
QueSZ11	364.26	0.0019	0.932
QueSZ12	432.56	0.0016	0.975
QueSZ01	461.40	0.0015	0.984

The corresponding $t_{1/2}$, photodegradation rate constant (k), and correlation coefficients (R^2) are summarized in Table 4. The relatively high R^2 values obtained for both free and encapsulated quercetin indicate that the degradation behaviour can be reasonably described using a first-order kinetic model. Comparison of the k values showed that free quercetin exhibited the fastest photodegradation rate under UV exposure, whereas quercetin encapsulated within the delivery systems displayed lower k values, indicating enhanced resistance to photodegradation. In addition, encapsulation within the delivery systems prolonged the $t_{1/2}$ of quercetin, demonstrating the protective effect against photodegradation. Systems with increasing zein content exhibited lower k values and longer $t_{1/2}$ values, suggesting improved photostability. This may be attributed to stronger hydrophobic interactions and the denser protein network associated with zein-rich matrices, which could provide more effective shielding against UV-induced degradation [85].

3.10. Antifeedant activity and feeding behaviour modulation

Antifeedant efficacy was evaluated through feeding preference bioassays using aphids as a model insect, with the AR used as the primary evaluation metric [49]. Positive AR values indicate antifeedant activity, whereas negative values indicate phagostimulatory effects. The 4 h observation period was selected as the primary evaluation window because aphids typically establish stable feeding behaviour within this period [49]. Among all formulations, delivery systems containing higher proportions of zein generally exhibited greater antifeedant performance, with QueSZ12 showing the highest efficacy across all tested

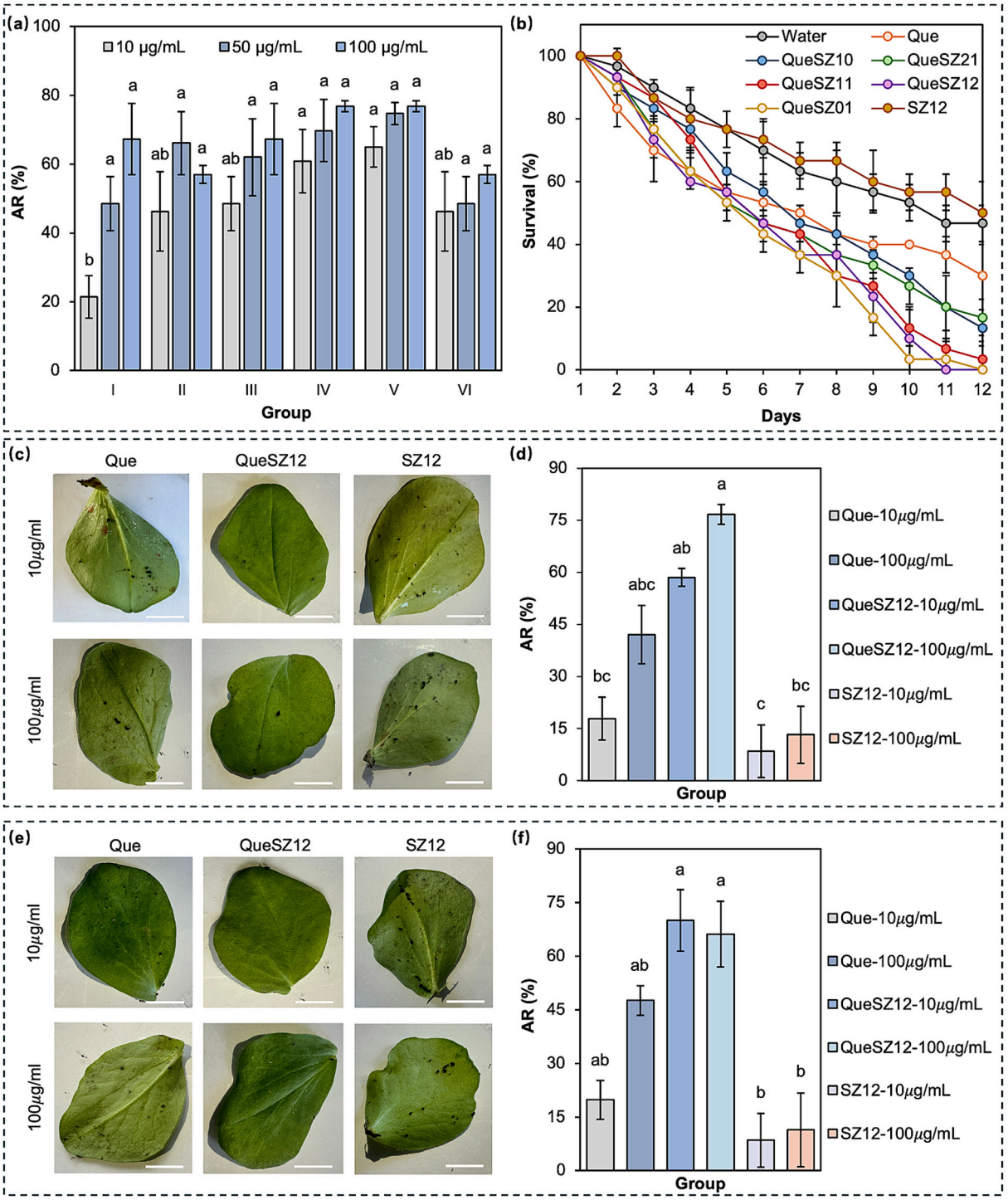

Fig. 8. Antifeedant efficacy and mortality of quercetin-loaded SPI-zein delivery systems. (a) Concentration-dependent AR of free quercetin and different quercetin-loaded SPI-zein delivery systems after 4 h exposure. Roman numerals (I-VI) correspond to quercetin, QueSZ10, QueSZ21, QueSZ11, QueSZ12, and QueSZ01, respectively. (b) Changes in the survival rate of aphids over 12 days. (c, d) Representative photographs and AR after 1 h exposure, and (e, f) after 8 h exposure, for quercetin, QueSZ12, and SZ12. Scale bars: 1.5 cm.

concentrations (Fig. 8a). Considering that zein provides the principal hydrophobic domains within the SPI-zein matrix, the superior performance of QueSZ12 may be associated with improved stabilisation and retention of the hydrophobic quercetin after deposition on the leaf surface. Such enhanced retention would be expected to maintain greater local availability of quercetin at aphid feeding sites, thereby strengthening feeding deterrence.

To further evaluate the temporal characteristics of the antifeedant response, additional observations were conducted at 1 h and 8 h to assess initial feeding inhibition and sustained deterrent activity, respectively (Fig. 8c-f). QueSZ12 exhibited both a rapid onset of antifeedant activity and persistent feeding deterrence throughout the 8 h observation period. In contrast, free quercetin produced a weaker and more delayed response, whereas SZ12 alone showed negligible activity, confirming that the antifeedant effect primarily originated from quercetin rather than the protein carrier. The sustained activity observed for

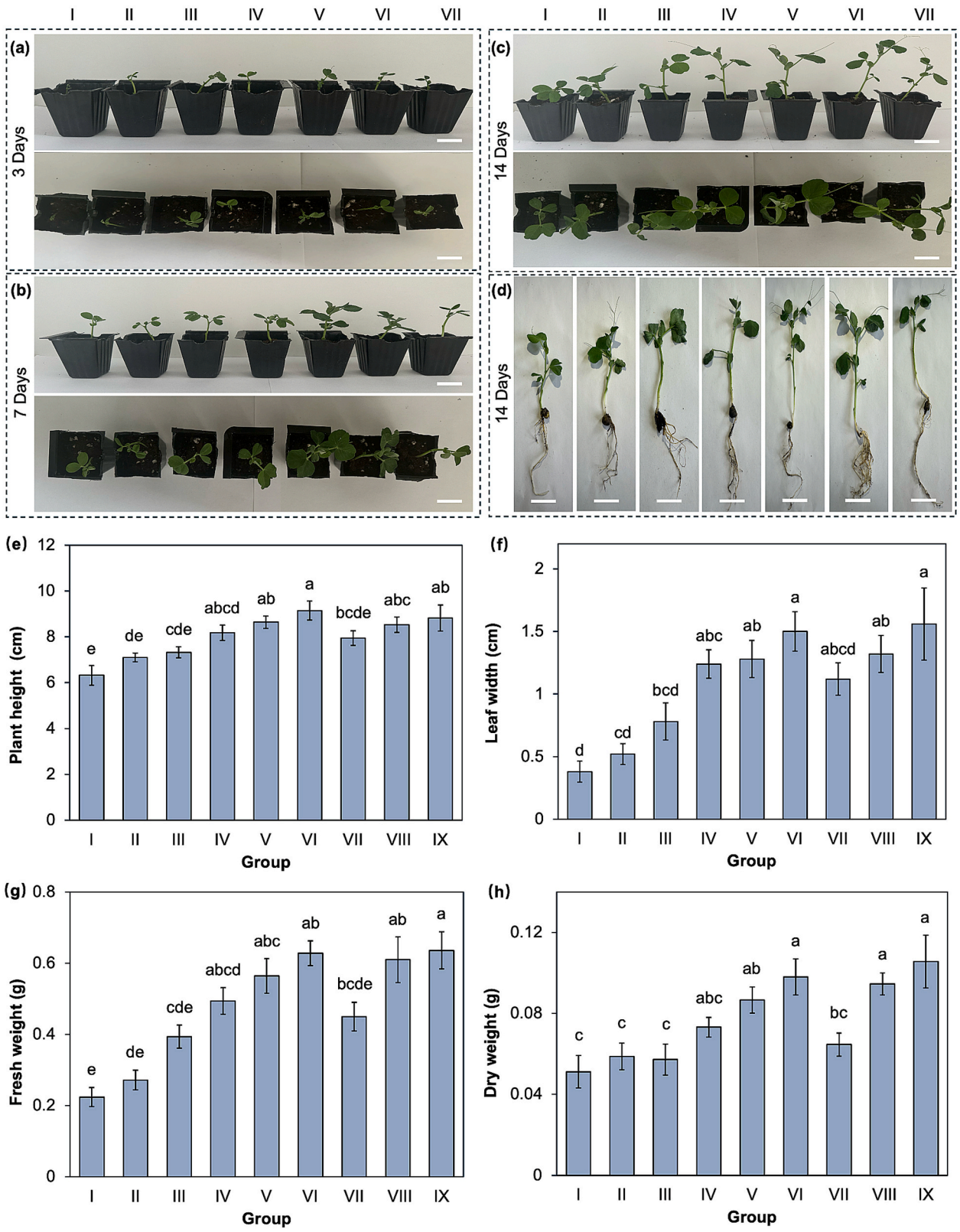

Fig. 9. Growth performance of pea seedlings treated with different formulations over time. Visual documentation of pea seedling development at (a) 3 days, (b) 7 days, (c) 14 days, and (d) overall plant morphology after 14 days. Scale bars: 2 cm. (e) Plant height, (f) leaf width, (g) fresh weight, and (h) dry weight of pea seedlings measured 14 days after treatment with different formulations. Roman numerals (I-IX) correspond to water, free quercetin, QueSZ10, QueSZ21, QueSZ11, QueSZ12, QueSZ01, SZ11, and SZ12, respectively.

QueSZ12 is also consistent with the controlled-release characteristics of the delivery system, suggesting that gradual release from the protein matrix may help maintain biologically effective concentrations of quercetin over time instead of relying solely on immediate availability following application. Interestingly, at both the 1 h and 8 h timepoints, increasing the application concentration of QueSZ12 did not produce a corresponding increase in antifeedant activity. One possible explanation is that adsorption of the formulation onto the leaf surface may approach saturation at higher application levels, thereby limiting further accumulation of quercetin at aphid feeding sites [86]. Similar concentration-dependent plateaus have been reported for other lipophilic antifeedant compounds [14,87]. Alternatively, once quercetin concentrations exceed the threshold required to elicit feeding deterrence, further increases in local concentration may contribute little additional behavioural response. Our results suggest the existence of an optimal concentration range beyond which increasing dosage does not substantially improve antifeedant efficacy.

The mortality profiles further demonstrated clear formulation-dependent effects during the 12-day observation period (Fig. 8b). The water-treated group maintained approximately 46.7% survival by day 12, while the SZ12-treated group showed only marginal differences (50% survival), confirming that the carrier itself exhibited negligible insecticidal activity. The relatively high mortality observed in these two control groups during the later stages of the experiment most likely reflects normal background mortality associated with prolonged maintenance under laboratory conditions rather than treatment-related effects. Nevertheless, separation between the quercetin-loaded formulations and both control groups was already evident at earlier timepoints, before substantial background mortality had accumulated, indicating that the enhanced mortality resulted from quercetin exposure rather than natural attrition. All quercetin-loaded SPI-zein delivery systems produced substantially greater cumulative mortality than the controls. Among them, QueSZ12 and QueSZ01 achieved complete mortality by days 11 and 12, respectively, whereas the remaining formulations reduced aphid survival to approximately 10% by day 12. Rather than inducing rapid acute toxicity, quercetin is generally considered to impair aphid feeding behaviour and disrupt normal physiological function, leading to progressive mortality under prolonged exposure [88]. From a delivery perspective, the delayed but sustained mortality profile is consistent with the controlled-release behaviour of the SPI-zein delivery system. By maintaining prolonged exposure to quercetin, rather than relying on a high initial burst, the formulation may provide continuous physiological stress that gradually reduces aphid survival over time. Collectively, these findings suggest that the enhanced biological performance of QueSZ12 arises not only from the intrinsic antifeedant activity of quercetin but also from improved delivery characteristics, including stabilisation of the bioactive compound and sustained release following application.

3.11. Plant growth-promoting effects of the quercetin-loaded SPI-zein delivery systems

The plant growth-promoting effects of the quercetin-loaded SPI-zein delivery systems were evaluated using pea seedlings as a model crop over a 14-day cultivation period (Fig. 9a-d). All formulations produced significantly greater plant growth than both the water control and free quercetin, particularly with respect to more developed root systems and increased leaf area. Measurements of plant height, leaf width, fresh weight, and dry weight consistently demonstrated substantial growth stimulation by the delivery systems (Fig. 9e-h). Among all formulations, QueSZ12 achieved the greatest plant height (9.14 ± 0.42 cm), followed by QueSZ11 (8.64 ± 0.27 cm) and QueSZ21 (8.18 ± 0.33 cm), all of which were significantly greater than both the water control (6.32 ± 0.43 cm) and free quercetin (7.10 ± 0.19 cm). Similar trends were observed for leaf width, with QueSZ12 producing the broadest leaves (1.50 ± 0.16 cm) compared with the water control (0.38 ± 0.08 cm). Fresh weight measurements likewise showed significant increases for QueSZ12 (0.63 ± 0.03 g) and QueSZ11 (0.56 ± 0.05 g), while dry weight analysis revealed increases of approximately 2–3 times relative to the water-treated group. These results indicate that the SPI-zein formulations not only function as delivery vehicles for quercetin but also provide additional agronomic benefits that promote plant development.

To further elucidate the origin of the growth-promoting effect, additional comparisons were performed using free quercetin and the unloaded SPI-zein carrier systems (Fig. S7 and S8). Free quercetin exhibited negligible effects on plant growth, whereas SZ12 produced growth responses comparable to those of QueSZ12. This direct comparison indicates that the observed growth promotion primarily originates from the protein carrier rather than from quercetin itself. Unlike conventional carrier materials that primarily serve passive encapsulation functions, the SPI-zein matrix therefore appears to contribute additional biological functionality beyond cargo delivery. A plausible explanation for this behaviour is the gradual biodegradation of SPI and zein in soil, during which amino acids, peptides, and nitrogen-containing degradation products are released and become available for plant utilisation [27,89]. Although soil nitrogen availability and degradation kinetics were not directly quantified in the present study, previous studies have demonstrated that protein-based agricultural formulations can enhance nutrient availability and promote plant growth through microbial decomposition [90,91].

4. Conclusions

This study developed a bioinspired pomegranate-like delivery system via spray drying, encapsulating quercetin within an SPI-zein matrix to achieve integrated pest management and plant growth promotion. The optimized formulation, QueSZ12, exhibited pH-responsive release behaviour together with favorable physicochemical stability, enhanced rainfastness, foliar adhesion, and storage performance. In agricultural applications, it significantly enhanced antifeedant activity against black bean aphids and promoted pea seedling growth. Future work should focus on elucidating the mechanistic basis of these multifunctional effects under agricultural conditions, as well as validating performance across diverse crop-pest systems under field environments, with particular attention to soil-microbial interactions. Although quercetin was used as a model bioactive compound in this study, our SPI-zein platform is not inherently limited to its encapsulation and may be extended to a broader range of natural actives, enabling modular design of multifunctional delivery systems. Overall, this study establishes a protein-based, property-tunable delivery strategy that integrates controlled release, crop protection, and plant growth regulation, offering a versatile platform for sustainable agricultural nanotechnology.

CRediT authorship contribution statement

Keke Xiao: Writing – review & editing, Writing – original draft, Visualization, Methodology, Investigation, Conceptualization. **Wing-Fu Lai:** Conceptualization, Methodology, Visualization, Formal analysis, Validation, Supervision, Writing – review & editing.

Declaration of competing interest

Authors declare that they have no competing interests.

Acknowledgments

Funding: Not applicable.

Appendix A. Supplementary data

Supplementary data to this article can be found online at https://doi.org/10.1016/j.jconrel.2026.115227.

Data availability

Data will be made available on request.

References

[1] N. Alexandratos, J. Bruinsma, World Agriculture Towards 2030/2050: The 2012 Revision, ESA Working Paper No. 12-03, Food and Agriculture Organization of the United Nations, 2012.
[2] J.W. Ding, L.N. Guo, S.H. Li, Q. Gao, W. Wu, D.Q. Li, J. Li, Bi-directional pH-responsive cellulose nanocrystals-based pesticide microcapsules for sustainable agriculture, Carbohydr. Polym. 368 (2025) 124242.
[3] E.W. Riddick, Evaluating the effects of flavonoids on insects: implications for managing pests without harming beneficials, Insects 15 (2024) 956.
[4] X. Jiang, F. Yang, W. Jia, Y. Jiang, X. Wu, S. Song, H. Shen, J. Shen, Nanomaterials and nanotechnology in agricultural pesticide delivery: a review, Langmuir 40 (2024) 18806–18820.
[5] R. Tao, C. You, Q. Qu, X. Zhang, Y. Deng, W. Ma, C. Huang, Recent advances in the design of controlled- and sustained-release micro/nanocarriers of pesticide, Environ. Sci. Nano 10 (2023) 351–371.
[6] G.L. Zabot, F. Schaefer Rodrigues, L. Polano Ody, M. Vinicius Tres, E. Herrera, H. Palacin, J.S. Cordova-Ramos, I. Best, L. Olivera-Montenegro, Encapsulation of bioactive compounds for food and agricultural applications, Polymers 14 (2022) 4194.
[7] V. Pereira, O. Figueira, P.C. Castilho, Flavonoids as insecticides in crop protection-a review of current research and future prospects, Plants 13 (2024) 776.
[8] E.W. Riddick, Potential of quercetin to reduce herbivory without disrupting natural enemies and pollinators, Agriculture 11 (2021) 476.
[9] S. Goławska, I. Łukasik, A.A. Chojnacki, Luteolin and quercetin affect aphid feeding behavior, Eur. Zool. J. 91 (2024) 318–331.
[10] J.E. Casida, K.A. Durkin, Neuroactive insecticides: targets, selectivity, resistance, and secondary effects, Annu. Rev. Entomol. 58 (2013) 99–117.
[11] R. Zhao, S. Hu, T. Chen, Y. Li, X. Chi, S. Yu, W. Wang, D. Liu, B. Zhu, J. Hu, Innovative delivery strategies for quercetin: a comprehensive review of advances and challenges, Compr. Rev. Food Sci. Food Saf. 24 (2025) e70146.
[12] K. Kandemir, M. Tomas, D.J. McClements, E. Capanoglu, Recent advances on the improvement of quercetin bioavailability, Trends Food Sci. Technol. 119 (2022) 192–200.
[13] R. Pavela, K. Kovarikova, M. Novak, Botanical antifeedants: an alternative approach to pest control, Insects 16 (2025) 136.
[14] X. Pan, X. Guo, T. Zhai, D. Zhang, W. Rao, F. Cao, X. Guan, Nanobiopesticides in sustainable agriculture: developments, challenges, and perspectives, Environ. Sci. Nano 10 (2023) 41–61.
[15] Y. Xiao, T. Ahmad, T. Belwal, R.M. Aadil, M. Siddique, L. Pang, Y. Xu, A review on protein based nanocarriers for polyphenols: interaction and stabilization mechanisms, Food Innov. Adv. 2 (2023) 193–202.
[16] E. Kianfar, Protein nanoparticles in drug delivery: animal protein, plant proteins and protein cages, albumin nanoparticles, J. Nanobiotechnol. 19 (2021) 159.
[17] E. Ma, Z. Fu, K. Chen, L. Sun, Y. Zhang, Z. Liu, L. Li, X. Guo, Smart protein-based fluorescent nanoparticles prepared by a continuous nanoprecipitation method for pesticides' precise delivery and tracing, J. Agric. Food Chem. 71 (2023) 8391–8399.
[18] K. Verma, C. Sarkar, S. Saha, Exploration of biodegradable polymeric particles in agriculture: a holistic approach for sustainable farming, Environ. Sci. Adv. 4 (2025) 409–431.
[19] D. Jao, Y. Xue, J. Medina, X. Hu, Protein-based drug-delivery materials, Materials 10 (2017) 517.
[20] A. Gomes, P. Sobral, Plant protein-based delivery systems: an emerging approach for increasing the efficacy of lipophilic bioactive compounds, Molecules 27 (2021) 60.
[21] C. Ferraro, M. Dattilo, F. Patitucci, S. Prete, G. Scopelliti, O.I. Parisi, F. Puoci, Exploring protein-based carriers in drug delivery: a review, Pharmaceutics 16 (2024) 1172.
[22] X. Xiao, P.R. Zou, F. Hu, W. Zhu, Z.J. Wei, Updates on plant-based protein products as an alternative to animal protein: technology, properties, and their health benefits, Molecules 28 (2023) 4016.
[23] S. Gupta, G. Ghoshal, Plant protein hydrogel as a delivery system of curcumin: characterization and in vitro release kinetics, Food Bioprod. Process. 143 (2024) 66–79.
[24] S. Jafarzadeh, M. Forough, S. Amjadi, V. Javan Kouzegaran, H. Almasi, F. Garavand, M. Zargar, Plant protein-based nanocomposite films: a review on the used nanomaterials, characteristics, and food packaging applications, Crit. Rev. Food Sci. Nutr. 63 (2023) 9667–9693.
[25] C.T.J. Ferguson, A.A. Al-Khalaf, R.E. Isaac, O.J. Cayre, pH-responsive polymer microcapsules for targeted delivery of biomaterials to the midgut of *Drosophila suzukii*, PLoS One 13 (2018) e0201294.
[26] D.X. Zhang, R. Wang, C. Ren, Y. Wang, B.X. Li, W. Mu, F. Liu, Y. Hou, One-step construct responsive lignin/polysaccharide/fe nano loading system driven by digestive enzymes of lepidopteran for precise delivery of pesticides, ACS Appl. Mater. Interfaces 14 (2022) 41337–41347.
[27] T. Zhang, H. Wang, C. Chen, Y. Wang, Z. Wang, M. Qi, C. Yuan, F. Liu, N. Zou, Bifunctional controlled-release pesticide delivery granule synchronizes pest control with plant health preservation, Chem. Eng. J. 523 (2025) 168634.
[28] N. Li, Z. Shen, S. Chen, Z. Wang, J. Luo, Multifunctional dual-structure carrier based on polyglutamic acid for enhanced precision and stability in foliar insecticide delivery, Chem. Eng. J. 524 (2025) 169693.
[29] P. Qin, T. Wang, Y. Luo, A review on plant-based proteins from soybean: health benefits and soy product development, J. Agric. Food Res. 7 (2022) 100265.
[30] S. Chen, C. Sun, Y. Wang, Y. Han, L. Dai, A. Abliz, Y. Gao, Quercetagetin-loaded composite nanoparticles based on zein and hyaluronic acid: formation, characterization, and physicochemical stability, J. Agric. Food Chem. 66 (2018) 7441–7450.
[31] Y. Wang, X. Wang, Binding, stability, and antioxidant activity of quercetin with soy protein isolate particles, Food Chem. 188 (2015) 24–29.
[32] Y. Zhang, R. Hou, B. Zhu, G. Yin, J. Zhang, W. Zhao, J. Zhang, T. Li, Z. Zhang, H. Wang, Z. Li, Changes on the conformational and functional properties of soybean protein isolate induced by quercetin, Front. Nutr. 9 (2022) 966750.
[33] H. Li, D. Wang, C. Liu, J. Zhu, M. Fan, X. Sun, T. Wang, Y. Xu, Y. Cao, Fabrication of stable zein nanoparticles coated with soluble soybean polysaccharide for encapsulation of quercetin, Food Hydrocoll. 87 (2019) 342–351.
[34] R. Paliwal, S. Palakurthi, Zein in controlled drug delivery and tissue engineering, J. Control. Release 189 (2014) 108–122.
[35] K. Koch, B. Bhushan, W. Barthlott, Multifunctional surface structures of plants: An inspiration for biomimetics, Prog. Mater. Sci. 54 (2009) 137–178.
[36] S. Chakraborty, D. Bera, L. Roy, C.K. Ghosh, Biomimetic and bioinspired nanostructures: recent developments and applications, in: M. Sen, M. Mukherjee (Eds.), Bioinspired and Green Synthesis of Nanostructures: A Sustainable Approach, Scrivener Publishing, 2023, pp. 353–404.
[37] W. Wagermaier, K. Razghandi, P. Fratzl, A bio-inspired perspective on materials sustainability, Adv. Mater. 37 (2025) e2413096.
[38] Q. Ye, F. Ge, Y. Wang, M.W. Woo, P. Wu, X.D. Chen, C. Selomulya, On improving bioaccessibility and targeted release of curcumin-whey protein complex microparticles in food, Food Chem. 346 (2021) 128900.
[39] P.K. Smith, R.I. Krohn, W. Barthlott, G.T. Hermanson, A.K. Mallia, F.H. Gartner, M. D. Provenzano, E.K. Fujimoto, N.M. Goeke, B.J. Olson, D.C. Klenk, Measurement of protein using bicinchoninic acid, Anal. Biochem. 150 (1985) 76–85.
[40] L.D. Daza, A. Fujita, C.S. Fávaro-Trindade, J.N. Rodrigues-Ract, D. Granato, M. I. Genovese, Effect of spray drying conditions on the physical properties of Cagaita (*Eugenia dysenterica* DC.) fruit extracts, Food Bioprod. Process. 97 (2016) 20–29.
[41] P. Wang, J. Wang, H. Hu, N. Ding, F. Wu, G. Fang, J. Mao, C. Wu, X. Liu, Encapsulation of quercetin in zein/sodium caseinate nanoparticles: fabrication, characterization, stability and controlled release properties, Food Res. Int. 230 (2026) 118608.
[42] Z. Sun, D. Li, P. Lin, Y. Zhao, J. Zhang, I. Sergeeva, Y. Li, H. Zheng, Preparation, characterization, and binding mechanism of quercetin-loaded composite nanoparticles based on zein-soybean protein isolate, Food Chem. 463 (2025) 141359.
[43] Y.e. Shi, X. Zhuang, L. Cao, S. Gou, Y. Xiong, W.F. Lai, Z. Wang, A.L. Rogach, Copper-nanocluster-based transparent ultraviolet-shielding polymer films, ChemNanoMat 5 (2018) 110–115.
[44] W.F. Lai, E.M. Huang, W.T. Wong, A gel-forming clusteroluminogenic polymer with tunable emission behavior as a sustained-release carrier enabling real-time tracking during bioactive agent delivery, Appl. Mater. Today 21 (2020) 100876.
[45] T. Santadkha, W. Skolpap, V. Thitapakorn, Diffusion modeling and in vitro release kinetics studies of curcumin-loaded superparamagnetic nanomicelles in cancer drug delivery system, J. Pharm. Sci. 111 (2022) 1690–1699.
[46] W.F. Lai, W.T. Wong, Property-tuneable microgels fabricated by using flow-focusing microfluidic geometry for bioactive agent delivery, Pharmaceutics 13 (2021) 787.
[47] W.F. Lai, O.S. Reddy, L. Law, H. Wu, W.T. Wong, A self-indicating and antibacterial gelatine-chitosan blended hydrogel enabling real-time quality control and sustained bioactive agent delivery, RSC Adv. 13 (2023) 11865–11873.
[48] A. Juptner, R. Scherliess, Spray dried formulations for inhalation-meaningful characterisation of powder properties, Pharmaceutics 12 (2019) 14.
[49] N. Prota, H.J. Bouwmeester, M.A. Jongsma, Comparative antifeedant activities of polygodial and pyrethrins against whiteflies (*Bemisia tabaci*) and aphids (*Myzus persicae*), Pest Manag. Sci. 70 (2014) 682–688.
[50] M.J. Teng, Y.S. Wei, T.G. Hu, Y. Zhang, K. Feng, M.H. Zong, H. Wu, Citric acid cross-linked zein microcapsule as an efficient intestine-specific oral delivery system for lipophilic bioactive compound, J. Food Eng. 281 (2020) 109993.
[51] J.V.M. Benetti, J.T. do Prado Silva, V.R. Nicoletti, SPI microgels applied to Pickering stabilization of O/W emulsions by ultrasound and high-pressure homogenization: rheology and spray drying, Food Res. Int. 122 (2019) 383–391.
[52] C. Yu, J. Shan, H. Ju, X. Chen, G. Xu, Y. Wu, Construction of a ternary composite colloidal structure of zein/soy protein isolate/sodium carboxymethyl cellulose to deliver curcumin and improve its bioavailability, Foods 12 (2023) 2692.
[53] A.W. Newman, S.M. Reutzel-Edens, G. Zografi, Characterization of the "hygroscopic" properties of active pharmaceutical ingredients, J. Pharm. Sci. 97 (2008) 1047–1059.
[54] I. De Marco, Zein microparticles and nanoparticles as drug delivery systems, Polymers 14 (2022) 2172.
[55] E. Oleandro, M. Stanzione, G.G. Buonocore, M. Lavorgna, Zein-based nanoparticles as active platforms for sustainable applications: recent advances and perspectives, Nanomaterials 14 (2024) 414.
[56] C. Wen, J. Zhang, H. Zhang, Y. Duan, New perspective on natural plant protein-based nanocarriers for bioactive ingredients delivery, Foods 11 (2022) 1701.
[57] Y. Qi, Z. Zhang, Y. Wang, Z. Wu, Z. Qin, Y. Zhou, X. Yang, Preparation and characterization of vitamin E microcapsules stabilized by Zein with different polysaccharides, Int. J. Biol. Macromol. 268 (2024) 131975.

[58] K. Sarabandi, P. Gharehbeglou, S.M. Jafari, Spray-drying encapsulation of protein hydrolysates and bioactive peptides: opportunities and challenges, Dry. Technol. 38 (2019) 577–595.
[59] Q. Ye, M.W. Woo, C. Selomulya, Modification of molecular conformation of spray-dried whey protein microparticles improving digestibility and release characteristics, Food Chem. 280 (2019) 255–261.
[60] A. Kumari, U. Ahuja, M.K. Pandey, A. Roy, Optimizing whole grain rice fortification using microwave-assisted screw conveying spraying and drying setup: exploring solution absorption, gelatinization, and micronutrient retention, Food Chem. 468 (2025) 142455.
[61] D.L. Yang, R.K. Liu, Y. Wei, Q. Sun, J.X. Wang, Micro-sized nanoaggregates: spray-drying-assisted fabrication and applications, Particuology 85 (2024) 22–48.
[62] S. Zellmer, G. Garnweitner, T. Breinlinger, T. Kraft, C. Schilde, Hierarchical structure formation of nanoparticulate spray-dried composite aggregates, ACS Nano 9 (2015) 10749–10757.
[63] C. Arpagaus, A. Collenberg, D. Rutti, E. Assadpour, S.M. Jafari, Nano spray drying for encapsulation of pharmaceuticals, Int. J. Pharm. 546 (2018) 194–214.
[64] X. Cao, J. Cao, T. Xu, L. Zheng, J. Dai, X. Zhang, T. Tian, K. Ren, X. Tong, H. Wang, L. Jiang, Construction of nanodelivery system based on the interaction mechanism between ultrasound-treated soybean whey protein and quercetin: structure, physicochemical stability and bioaccessibility, Ultrason. Sonochem. 112 (2025) 107195.
[65] T. Yang, G. Qiao, X.W. Chen, Fabrication of complex interface and pH-switchable Pickering emulsions prepared by electrostatic associative of zein nanoparticles with QS-coated nanodroplets, Food Hydrocoll. 170 (2026) 111737.
[66] P. Alugoju, D. Narsimulu, J.U. Bhanu, N. Satyanarayana, L. Periyasamy, Role of quercetin and caloric restriction on the biomolecular composition of aged rat cerebral cortex: an FTIR study, Spectrochim. Acta A Mol. Biomol. Spectrosc. 220 (2019) 117128.
[67] F. Jin, Z. Xie, H. Zhang, M. Pang, S. Liu, B. Tian, Z. Feng, Development of zein-soy protein isolate-rutin supramolecular nanoparticles via pH-ultrasound-shifting method: structural characterization, stability, and gastrointestinal bioaccessibility, Food Chem. 506 (2026) 148194.
[68] Y. Luo, B. Zhang, M. Whent, L.L. Yu, Q. Wang, Preparation and characterization of zein/chitosan complex for encapsulation of α-tocopherol, and its in vitro controlled release study, Colloids Surf. B: Biointerfaces 85 (2011) 145–152.
[69] C. Qiu, Z. Zhang, X. Li, S. Sang, D.J. McClements, L. Chen, J. Long, A. Jiao, X. Xu, Z. Jin, Co-encapsulation of curcumin and quercetin with zein/HP-β-CD conjugates to enhance environmental resistance and antioxidant activity, npj Sci. Food 7 (2023) 29.
[70] P. Klitou, E. Parisi, S. Bordignon, F. Bravetti, I. Rosbottom, M. Dell'Aera, C. Cuocci, M.R. Chierotti, A. Altomare, E. Simone, Navigating the complex solid form landscape of the quercetin flavonoid molecule, Cryst. Growth Des. 23 (2023) 6034–6045.
[71] J. Liu, Y. Zhang, W. Liu, B. Gao, L.L. Yu, A novel zein-based composite nanoparticles for improving bioaccessibility and anti-inflammatory activity of resveratrol, Foods 10 (2021) 2773.
[72] M. Karaaslan, F. Sengun, U. Cansu, B. Basyigit, H. Saglam, A. Karaaslan, Gum arabic/maltodextrin microencapsulation confers peroxidation stability and antimicrobial ability to pepper seed oil, Food Chem. 337 (2021) 127748.
[73] C. Tsioptsias, I. Tsivintzelis, On the thermodynamic thermal properties of quercetin and similar pharmaceuticals, Molecules 27 (2022) 6630.
[74] L. Chen, M. Subirade, Elaboration and characterization of soy/zein protein microspheres for controlled nutraceutical delivery, Biomacromolecules 10 (2009) 3327–3334.
[75] H. Zhao, S. Wang, X. Liu, G. Zhao, L. Yang, H. Song, G. Zhang, Y. He, H. Liu, Application of soy protein isolate fiber and soy soluble polysaccharide non-covalent complex: a potential way for pH-triggered release, Food Chem. 402 (2023) 134494.
[76] P.T. Cristofoletti, A.F. Ribeiro, C. Deraison, Y. Rahbe, W.R. Terra, Midgut adaptation and digestive enzyme distribution in a phloem feeding insect, the pea aphid *Acyrthosiphon pisum*, J. Insect Physiol. 49 (2003) 11–24.
[77] M. Hu, N. Reichholf, Y. Xia, L. Alvarez, X. Cao, S. Ma, A.J. deMello, L. Isa, Multi-compartment supracapsules made from nano-containers towards programmable release, Mater. Horiz. 9 (2022) 1641–1648.
[78] D. Zhao, N. Yang, Y. Wei, Q. Jin, Y. Wang, H. He, Y. Yang, B. Han, S. Zhang, D. Wang, Sequential drug release via chemical diffusion and physical barriers enabled by hollow multishelled structures, Nat. Commun. 11 (2020) 4450.
[79] F. Wang, Z. Hu, C. Abarca, M. Fefer, J. Liu, M.A. Brook, R. Pelton, Factors influencing agricultural spray deposit structures on hydrophobic surfaces, Colloids Surf. A Physicochem. Eng. Asp. 553 (2018) 288–294.
[80] L. Xu, P. He, Y. Duan, Z. Yu, F. Yang, Synergy of different leaf traits determines the particulate matter retention capacity and its susceptibility to rain wash-off, Sci. Total Environ. 906 (2024) 167365.
[81] H. Zhang, T. Zhang, X. Zhang, J. Xu, X. Peng, S. Guo, Powder-level mechanisms of soy protein isolate functional deterioration during storage: the interplay of aggregation and oxidative stress, Food Chem. 495 (2025) 146513.
[82] Z. Zhang, Y. Hu, H. Ji, Q. Lin, X. Li, S. Sang, D. Julian McClements, L. Chen, J. Long, A. Jiao, X. Xu, Z. Jin, C. Qiu, Physicochemical stability, antioxidant activity, and antimicrobial activity of quercetin-loaded zein nanoparticles coated with dextrin-modified anionic polysaccharides, Food Chem. 415 (2023) 135736.
[83] C.K. Curi-Borda, V. Tannira, N. Gentile, J.A. Alvarado, B. Bergenståhl, Model for measuring light stability of photolabile substances in powder beds using spray dried bixin microcapsules, Colloids Surf. A Physicochem. Eng. Asp. 627 (2021) 127131.
[84] M.H.G. Gomes, L.E. Kurozawa, Surface composition and microstructure of spray-dried microparticles: a review about their effect on functional properties, Dry. Technol. 42 (2024) 1665–1682.
[85] C. Xia, W. Wang, L. Wang, H. Liu, J. Xiao, Multilayer zein/gelatin films with tunable water barrier property and prolonged antioxidant activity, Food Packag. Shelf Life 19 (2019) 76–85.
[86] S. Gupta, A. Roy, Deciphering the role of phytoanticipins, phytoalexins, and polyphenols in plant-insect defense, in: I.K. Singh, A. Singh (Eds.), Plant-Pest Interactions: From Molecular Mechanisms to Chemical Ecology, Springer, 2021, pp. 305–335.
[87] O. Koul, Phytochemicals and insect control: an antifeedant approach, Crit. Rev. Plant Sci. 27 (2008) 1–24.
[88] K. Stec, B. Kordan, B. Gabrys, Quercetin and rutin as modifiers of aphid probing behavior, Molecules 26 (2021) 3622.
[89] D. Geisseler, W.R. Horwath, Relationship between carbon and nitrogen availability and extracellular enzyme activities in soil, Pedobiologia 53 (2009) 87–98.
[90] J.P. Schimel, J. Bennett, Nitrogen mineralization: challenges of a changing paradigm, Ecology 85 (2004) 591–602.
[91] E. Kebede, Contribution, utilization, and improvement of legumes-driven biological nitrogen fixation in agricultural systems, Front. Sustain. Food Syst. 5 (2021) 767998.